Inorganic Chemistry
Article

*Inorg. Chem.* **2009**, *48*, 10757–10768 **10757**
DOI: 10.1021/ic901647n

# Copper Halide-Incorporated Tellurium−Iron Carbonyl Complexes: Transformation, Electrochemical Properties, and Theoretical Calculations

**Bo-Gaun Chen, Chia-Hua Ho, Chang-Ju Lee, and Minghuey Shieh***

*Department of Chemistry, National Taiwan Normal University, Taipei 116, Taiwan, Republic of China*

Received August 18, 2009

When the tellurium-capped tri-iron carbonyl cluster $[Et_4N]_2[TeFe_3(CO)_9]$ was treated with 1 equiv of CuX in THF at 0 °C, CuX-incorporated clusters $[Et_4N]_2[TeFe_3(CO)_9CuX]$ (X= Cl, $[Et_4N]_2$[**1a**]; Br, $[Et_4N]_2$[**1b**]; I, $[Et_4N]_2$[**1c**]) were formed, respectively. X-ray analysis showed that **1a**−**1c** each exhibited a $TeFe_3$ core with one Fe−Fe bond bridged by one CuX fragment. When the reactions were carried out at a molar ratio of 1:2 (X= Cl, Br) or 1:3 (X= I) in tetrahydrofuran (THF) or MeCN at 0 °C, $Cu_2X_2$-incorporated clusters $[Et_4N]_2[TeFe_3(CO)_9Cu_2X_2]$ (X= Cl, $[Et_4N]_2$[**2a**]; Br, $[Et_4N]_2$[**2b**]; I, $[Et_4N]_2$[**2c**]) were obtained, respectively. Cluster **2a** was structurally characterized by X-ray analysis to display a $TeFe_3$ core, in which one $TeFe_2$ plane was asymmetrically bridged and capped by one $\mu_3$-CuCl and another $\mu_4$-CuCl with two Cu atoms bonded. Complexes **1a**−**1c** underwent skeleton expansion to form $Cu_3X$-incorporated di-$TeFe_3$ clusters $[\{TeFe_3(CO)_9\}_2Cu_3X]^{2-}$ (X= Cl, **3a**; Br, **3b**; I, **3c**), respectively, upon treatment with 1 equiv of $[Cu(MeCN)_4][BF_4]$ at 0 °C. X-ray analysis showed that **3b** and **3c** each consisted of two $TeFe_3$ clusters that were linked by a $Cu_3X$ moiety. However, a similar reaction for **1a** and **1b** with 1 equiv of $[Cu(MeCN)_4][BF_4]$ at room temperature produced $Cu_4X_2$-linked di-$TeFe_3$ clusters $[\{TeFe_3(CO)_9\}_2Cu_4X_2]^{2-}$ (X= Cl, **4a**; Br, **4b**). Cluster **4a** was shown by X-ray analysis to have two $TeFe_3$ cores linked by a $Cu_4Cl_2$ moiety. Clusters **4a** and **4b** were also produced directly from the reaction of $[Et_4N]_2[TeFe_3(CO)_9]$ with 4 equiv of CuX (X= Cl, Br) in THF. Furthermore, the nature, the formation, the cluster transformation, and the electrochemistry of the CuX-incorporated mono- or di-$TeFe_3$ clusters are explained in terms of the effects of tellurium, copper halide, and the size of the metal skeleton, all of which are elucidated by molecular calculations at the B3LYP level of density functional theory.

## Introduction

Chalcogen-containing transition metal complexes have drawn increased attention in recent years, mainly because of their unusual structures and novel chemical reactivities, as well as for their close relationship with material science and catalysis.[1] In contrast to sulfur- and selenium-transition metal complexes, tellurium-containing transition metal complexes have attracted much attention, particularly because of the pronounced effect of the Te element on the entire metal skeleton.[2,3] However, study into the potential use of tellurium as a stabilizing ligand for metal clusters has been limited, and its use in their formation has been scarce. Previous studies on tellurium-containing iron carbonyl clusters have focused on their synthesis and structural features.[3−6] Thus, the ability of these complexes to function as building blocks for metal expansion reactions in terms of the effect of tellurium and transition metals is of great interest and is a challenge because of their potential uses in the preparation of mixed metal nanoparticles in nanotechnology.[7]

*To whom correspondence should be addressed. E-mail: mshieh@ntnu.edu.tw.

(1) (a) *The Chemistry of Metal Cluster Complexes*; Shriver, D. F., Kaesz, H. D., Adams, R. D., Eds.; Wiley-VCH Publishers: New York, 1990. (b) *Metal Clusters in Chemistry*; Braunstein, P., Oro, L. A., Raithby, P. R., Eds.; Wiley-VCH Publishers: Weinheim, 1999.

(2) (a) Herrmann, W. A. *Angew. Chem., Int. Ed. Engl.* **1986**, *25*, 56. (b) Ansari, M. A.; Ibers, J. A. *Coord. Chem. Rev.* **1990**, *100*, 223. (c) Dehnen, S.; Eichhöfer, A.; Fenske, D. *Eur. J. Inorg. Chem.* **2002**, 279.

(3) (a) Roof, L. C.; Kolis, J. W. *Chem. Rev.* **1993**, *93*, 1037. (b) Mathur, P. *Adv. Organomet. Chem.* **1997**, *41*, 243. (c) Compton, N. A.; Errington, R. J.; Norman, N. C. *Adv. Organomet. Chem.* **1990**, *31*, 91. (d) Kanatzidis, M. G.; Huang, S.-P. *Coord. Chem. Rev.* **1994**, *130*, 509. (e) Mathur, P.; Singh, A. K.; Mohanty, J. R.; Chatterjee, S.; Mobin, S. M. *Organometallics* **2008**, *27*, 5094.

(4) Bachman, R. E.; Whitmire, K. H. *Inorg. Chem.* **1994**, *33*, 2527.

(5) (a) Roof, L. C.; Smith, D. M.; Drake, G. W.; Pennington, W. T.; Kolis, J. W. *Inorg. Chem.* **1995**, *34*, 337. (b) Bachman, R. E.; Whitmire, K. H.; van Hal, J. *Organometallics* **1995**, *14*, 1792. (c) Konchenko, S. N.; Pushkarevsky, N. A.; Scheer, M. *J. Cluster Sci.* **2003**, *14*, 299. (d) Pushkarevsky, N. A.; Konchenko, S. N.; Scheer, M. *J. Cluster Sci.* **2007**, *18*, 606.

(6) (a) Shieh, M.; Chen, P.-F.; Peng, S.-M.; Lee, G.-H. *Inorg. Chem.* **1993**, *32*, 3389. (b) Shieh, M.; Chen, P.-F.; Peng, S.-M.; Lee, G.-H. *J. Chin. Chem. Soc.* **1994**, *41*, 151. (c) Shieh, M.; Shieh, M.-H. *Organometallics* **1994**, *13*, 920. (d) Shieh, M.; Chen, P.-F.; Tsai, Y.-C.; Shieh, M.-H.; Peng, S.-M.; Lee, G.-H. *Inorg. Chem.* **1995**, *34*, 2251. (e) Shieh, M.; Tang, T.-F.; Peng, S.-M.; Lee, G.-H. *Inorg. Chem.* **1995**, *34*, 2797. (f) Huang, K.-C.; Shieh, M.-H.; Jang, R.-J.; Peng, S.-M.; Lee, G.-H.; Shieh, M. *Organometallics* **1998**, *17*, 5202. (g) Shieh, M. *J. Cluster Sci.* **1999**, *10*, 3. (h) Shieh, M.; Lai, Y.-W. *J. Chin. Chem. Soc.* **2002**, *49*, 851. (i) Shieh, M.; Chen, H.-S.; Lai, Y.-W. *Organometallics* **2004**, *23*, 4018. (j) Shieh, M.; Ho, C.-H. *C. R. Chimie* **2005**, *8*, 1838.

(7) Femoni, C.; Iapalucci, M. C.; Kaswalder, F.; Longoni, G.; Zacchini, S. *Coord. Chem. Rev.* **2006**, *250*, 1580.

© 2009 American Chemical Society
Published on Web 10/15/2009

**Scheme 1**

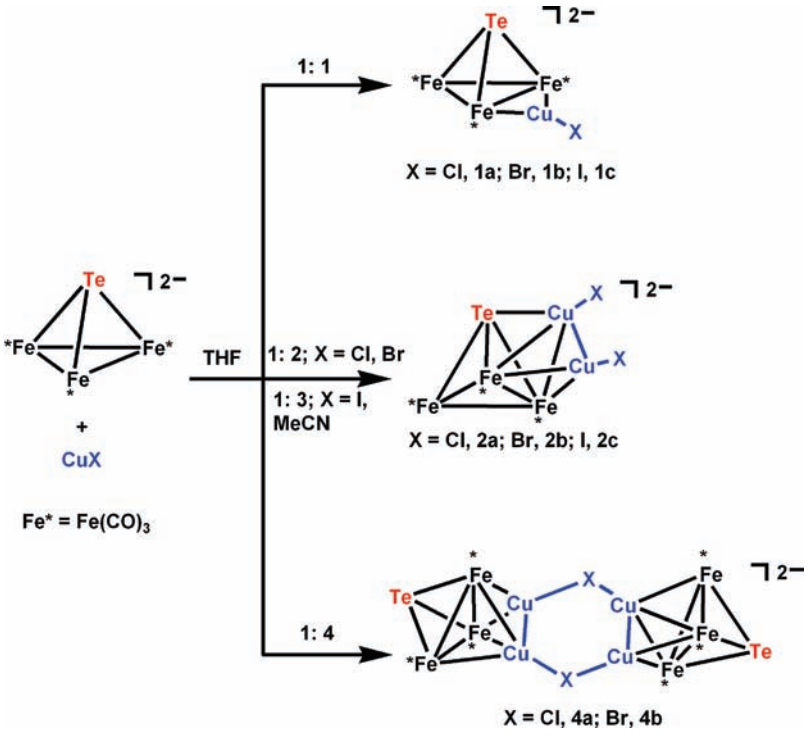


The previous study showed that the tellurium-capped tri-iron carbonyl complex, $[TeFe_3(CO)_9]^{2-}$,[4] exhibited an interesting affinity toward organic and inorganic electrophiles.[5,6f−6j] Recently, we have reported a series of copper halide-incorporated triiron selenide carbonyl clusters from the reaction of $[SeFe_3(CO)_9]^{2-}$ with CuX (X = Cl, Br, I).[8] Along this line, we attempted to extend our work[6] into whether $[TeFe_3(CO)_9]^{2-}$ could be used as a building unit for further metal expansion reactions. It has been shown that $[TeFe_3(CO)_9]^{2-}$ can be linked by $Cu^+$ cations to give a novel ternary semiconducting Te−Fe−Cu polymer.[9] To pursue the main-group element and the linker effects, the reactions of $[TeFe_3(CO)_9]^{2-}$ with various amounts of CuX (X = Cl, Br, I) have been systematically studied to probe the complicated coupling effect of tellurium and iron atoms in terms of different copper halides. In this study, we describe a rational route to a new series of CuX-, $Cu_2X_2$-, $Cu_3X$-, or $Cu_4X_2$-incorporated nanosized mono- or di-$TeFe_3$ carbonyl clusters. Also, with the aid of molecular calculations at the B3LYP level of density functional theory, the present study further pursues the nature, the structural transformation, and the electrochemistry of the resultant Te−Fe−Cu clusters in terms of the effects of copper halide and the size of the metal skeleton.

## Results and Discussion

**Reaction of $[Et_4N]_2[TeFe_3(CO)_9]$ with 1 equiv of CuX (X = Cl, Br, I).** When the tellurium-capped tri-iron cluster $[TeFe_3(CO)_9]^{2-}$ was treated with 1 equiv of CuX (X = Cl, Br, I) in tetrahydrofuran (THF) in an ice−water bath, mono-CuX-$TeFe_3$ clusters $[TeFe_3(CO)_9CuX]^{2-}$ (X = Cl, **1a**; Br, **1b**; I, **1c**) were produced, respectively, in good yields (Scheme 1). X-ray analysis showed that **1a**−**1c** each exhibited a $TeFe_3$ core with each Fe atom coordinated by three terminal carbonyls, in which one Fe−Fe bond was further bridged by one CuX fragment (X = Cl, **1a**; Br, **1b**; I, **1c**) (Figure 1, Supporting Information, Figures S1 and S2). These structures are structurally similar to their Se analogue $[SeFe_3(CO)_9CuX]^{2-}$ (X = Cl, Br, I).[8] The IR absorptions ($\nu_{CO}$) of **1a**−**1c** are shifted to lower energies as compared to their corresponding Se analogue, probably

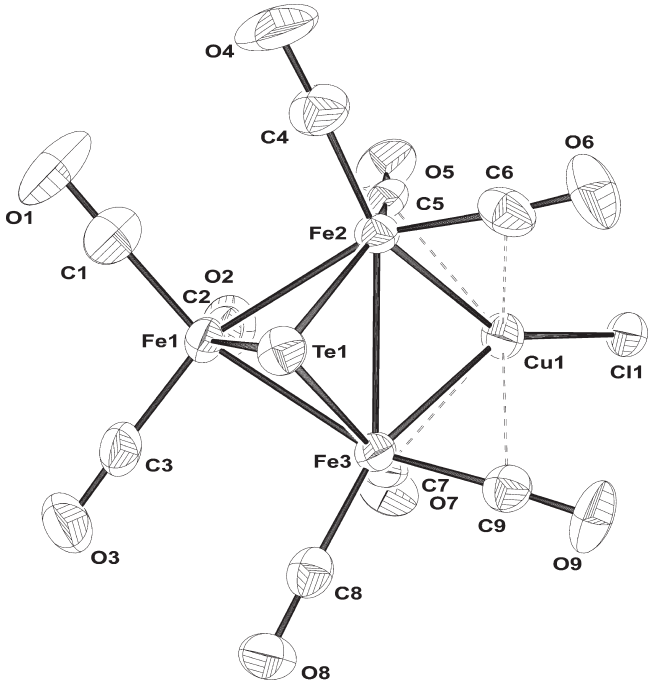


**Figure 1.** ORTEP diagram showing the structure and atom labeling for **1a**, showing 30% probability thermal ellipsoids.

(8) Shieh, M.; Miu, C.-Y.; Lee, C.-J.; Chen, W.-C.; Chu, Y.-Y.; Chen, H.-L. *Inorg. Chem.* **2008**, *47*, 11018.
(9) Shieh, M.; Ho, C.-H.; Sheu, W.-S.; Chen, B.-G.; Chu, Y.-Y.; Miu, C.-Y.; Liu, H.-L.; Shen, C.-C. *J. Am. Chem. Soc.* **2008**, *130*, 14114.

because of the better electron delocalization of Te versus Se onto the $Fe_3$ ring.

**Reaction of $[Et_4N]_2[TeFe_3(CO)_9]$ with 2 equiv of CuX (X = Cl, Br) or 3 equiv of CuI.** If $[TeFe_3(CO)_9]^{2-}$ was further treated with 2 equiv of CuX (X = Cl, Br) in THF or with 3 equiv of CuI in MeCN in an ice−water bath, $Cu_2X_2$-incorporated $TeFe_3$ clusters $[TeFe_3(CO)_9Cu_2X_2]^{2-}$ (X = Cl, **2a**; Br, **2b**; I, **2c**) were obtained, respectively, in good yields (Scheme 1). Clusters **2a**−**2c** were characterized by spectroscopic methods and elemental analysis. Cluster **2a** was further structurally characterized by X-ray analysis to consist of a $TeFe_3(CO)_9$ cluster with one Fe−Fe edge bridged by one Cu atom in which the $TeFe_2Cu$ butterfly was further capped by another Cu atom with the two Cu atoms covalently bonded and each externally bound to one Cl atom (Figure 2). Cluster **2a** can also be viewed to display a Cu-capped $TeFe_3Cu$ trigonal bipyramidal core geometry with one $\mu_4$-CuX occupying the axial position and another $\mu_3$-CuX capping the $Fe_2Cu$ triangle. Clusters **2b** and **2c** were believed to be isostructural with **2a** because of their IR absorption patterns similar to that of cluster **2a**, which is different from those observed for the $Fe_3-Cu_2X_2$-incorporated clusters $[SeFe_3(CO)_9Cu_2X_2]^{2-}$ (X = Cl, Br)[8] (Supporting Information, Figure S3).

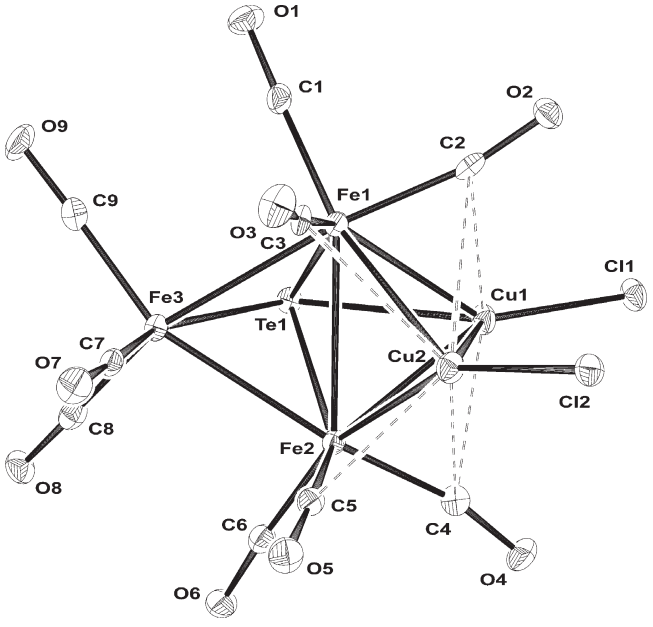


**Figure 2.** ORTEP diagram showing the structure and atom labeling for **2a**, showing 30% probability thermal ellipsoids.

**Reaction of $[Et_4N]_2[TeFe_3(CO)_9]$ with 4 equiv of CuX (X=Cl, Br).** Further investigation focused on the employment of $[TeFe_3(CO)_9]^{2-}$ as a building block with an increased amount of CuX to form the $TeFe_3$-based expanded framework. Results showed that if $[TeFe_3(CO)_9]^{2-}$ were treated with 4 equiv of CuX in THF at room temperature, $Cu_4X_2$-linked di-$TeFe_3$ clusters $[\{TeFe_3(CO)_9\}_2Cu_4X_2]^{2-}$ (X = Cl, **4a**; Br, **4b**) were formed, respectively, in good yields (Scheme 1). Clusters **4a** and **4b** were structurally analogous to one another based on the similar IR absorption patterns and their formulations were further substantiated by elemental analysis. X-ray analysis showed that **4a** consisted of two $TeFe_3(CO)_9$ clusters each bridged and capped by two covalently bonded Cu atoms in which the two $TeFe_3Cu_2$ clusters were further connected by two Cl atoms (Figure 3). The formation of $Cu_4X_2$-linked di-$TeFe_3$ clusters **4a** and **4b** were considered a result of the coupling reaction of **2a** or **2b** with the elimination of 2 equiv of $X^-$ (X = Cl, Br). Therefore, an excess amount of CuX (X = Cl, Br) used in this case functioned as the oxidizing agent to induce the dimerization of **2a** or **2b**. However, a similar reaction with CuI failed to give the analogous complex $[\{TeFe_3(CO)_9\}_2Cu_4I_2]^{2-}$ (**4c**) because of its poor stability compared to **4a** and **4b**. This phenomenon was further supported by density functional theory (DFT) calculations (discussed later).

**Structural Transformation of 1a−1c, 2a−2c, 3a−3c, 4a, and 4b.** Since CuX-, $Cu_2X_2$-, and $Cu_4X_2$-incorporated mono- or di-$TeFe_3$-based clusters were accomplished by fine-tuning the ratios of $[TeFe_3(CO)_9]^{2-}$ and CuX (X = Cl, Br, I), the controlled stepwise construction of these $TeFe_3$-based frameworks was further investigated and successfully achieved (Scheme 2).

As expected, when mono-CuX-$TeFe_3$ clusters **1a**−**1c** were treated with 1 equiv of CuX in THF (X = Cl, Br) or 2

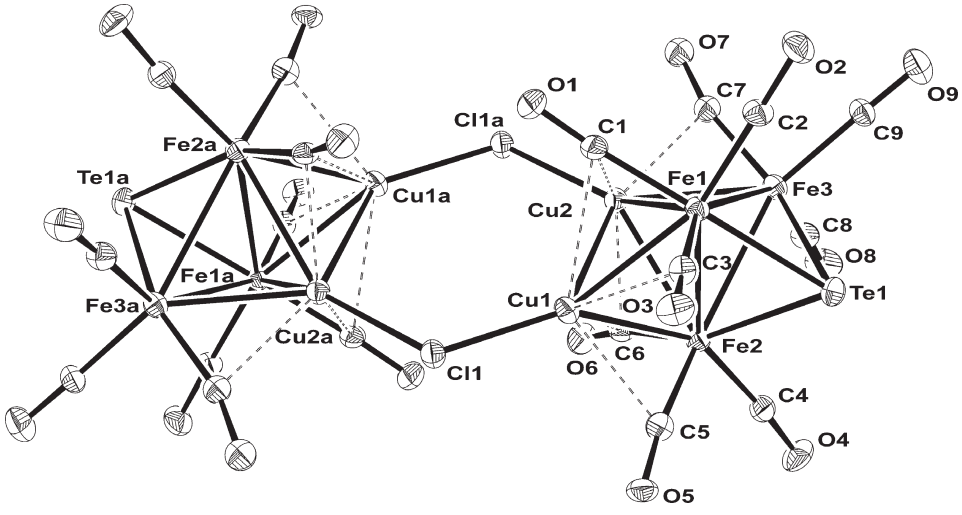


**Figure 3.** ORTEP diagram showing the structure and atom labeling for **4a**, showing 30% probability thermal ellipsoids.

**Scheme 2**

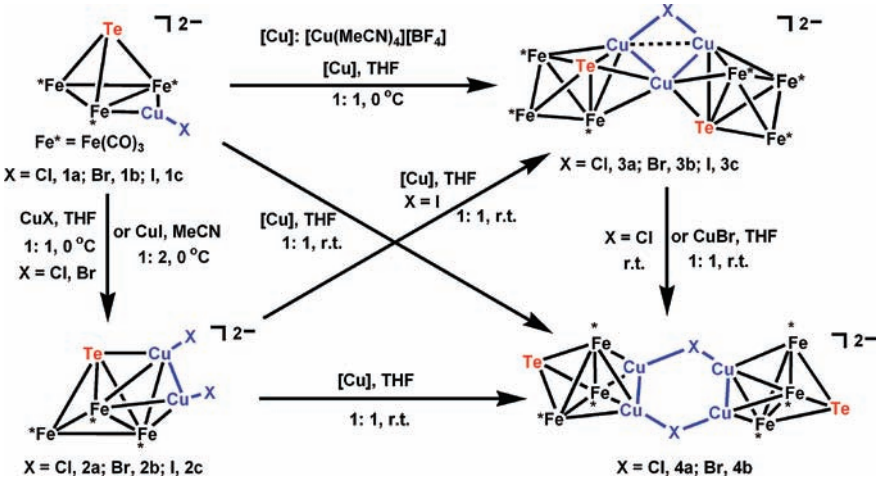


equiv of CuI in MeCN at 0 °C, $Cu_2X_2$-incorporated $TeFe_3$ clusters **2a**−**2c** were produced, respectively, in good yields. On the other hand, if clusters **1a** and **1b** were treated with 1 equiv of $[Cu(MeCN)_4][BF_4]$ in THF at room temperature, $Cu_4X_2$-linked di-$TeFe_3$ complexes **4a** and **4b** were obtained, respectively. In contrast, if a similar reaction of complexes **1a**−**1c** with 1 equiv of $[Cu(MeCN)_4][BF_4]$ in THF was carried out at 0 °C, the new $Cu_3X$-incorporated di-$TeFe_3$ clusters $[\{TeFe_3(CO)_9\}_2Cu_3X]^{2-}$ (X = Cl; **3a**; Br, **3b**; I, **3c**) were produced. X-ray analysis showed that clusters **3b** and **3c** each consisted of two $TeFe_3$ clusters that were further linked by a $Cu_3X$ moiety (X = Br, **3b**; I, **3c**) (Figure 4 and Supporting Information, Figure S4). However, cluster **3a** was only observed spectroscopically and is believed to be structurally similar to **3b** and **3c** because of their similar IR absorption patterns. The poor stability of **3a** is also supported by DFT calculations and will be discussed later. The kinetic product **3a** was found to quickly transform to its thermodynamic product **4a** at room temperature while cluster **3b** coupled with 1 equiv of CuBr in THF at room temperature to give cluster **4b**. However, cluster **3c** failed to form the analogous **4c** under similar conditions because of the poor stability of **4c** (discussed later).

In addition, $Cu_2X_2$-incorporated clusters **2a** and **2b** could undergo dimerization to give $Cu_4X_2$-linked di-$TeFe_3$clusters **4a** and **4b**, respectively, upon treatment with 1 equiv of $[Cu(MeCN)_4][BF_4]$ in THF at room temperature, through oxidative coupling processes via a loss of halide. Unlike the cases for **2a** and **2b**, when **2c** reacted with 1 equiv of $[Cu(MeCN)_4][BF_4]$ in THF at room temperature, the $Cu_3I$-incorporated di-$TeFe_3$ complex **3c** was formed as the final product with no observation of the $Cu_4I_2$-linked di-$TeFe_3$ product because of the poor stability of **4c** compared to **4a** and **4b**. It is also of great interest to note that cluster **4b** could be produced from cluster **1b** via the stepwise addition of $[Cu(MeCN)_4][BF_4]$ and CuBr, regardless of the addition order, with the formation of either cluster **2b** or cluster **3b** as the intermediate.

**Structural Comparison of 1a−1c, 2a, 3b, 3c, and 4a.** According to the single-crystal X-ray analysis, complexes **1a**−**1c** and **2a** displayed either the CuX- or $Cu_2X_2$-incorporated $TeFe_3$-based structures while complexes **3b**, **3c**, and **4a** exhibited either $Cu_3X$- or $Cu_4X_2$-incorporated

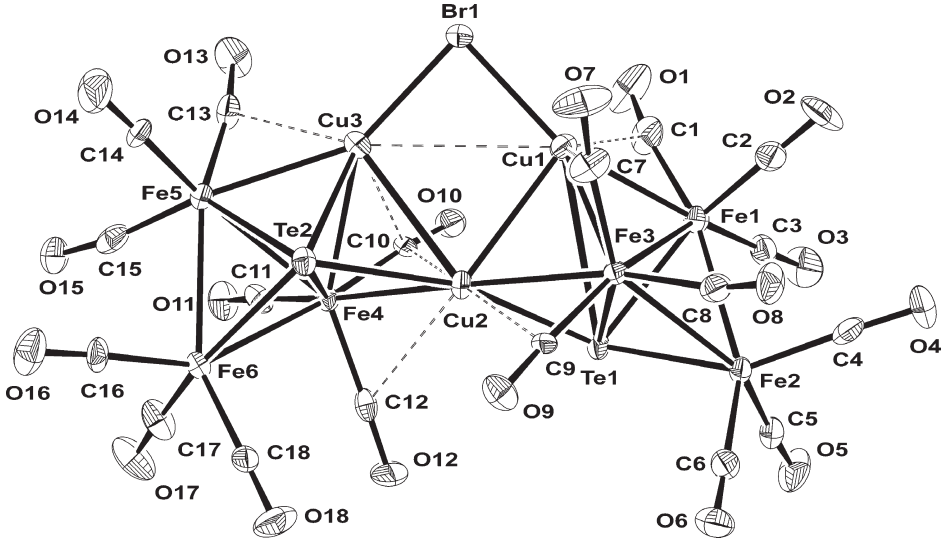


**Figure 4.** ORTEP diagram showing the structure and atom labeling for **3b**, showing 30% probability thermal ellipsoids.

di-$TeFe_3$-based structures. These clusters reached a range of nanosized regions of approximately 0.81 nm (CuX-$TeFe_3$ core), 0.84 nm ($Cu_2X_2$-$TeFe_3$ core), 1.37 nm ($Cu_3X$-di-$TeFe_3$ core), and 1.50 nm ($Cu_4X_2$-di-$TeFe_3$ core).

Clusters **1a**−**1c** were isostructural species and each displayed a $TeFe_3$ tetrahedral geometry with one $\mu_3$-Te atom and one Fe−Fe bond bridged by one CuX (X = Cl, Br, I) fragment (Figure 1, Supporting Information, Figures S1 and S2). Complexes **1a** and **1b** each contained two independent but chemically similar asymmetric anions in the unit cell, which were similar in bond distances and angles−only one structure is described for comparison. $[Et_4N]_2$[**1a**] was structurally similar to the previously reported $[PPN]_2$[**1a**],[5b] but with different cations. In addition, $Cu_2Cl_2$-incorporated $TeFe_3$ cluster **2a** had a $TeFe_3(CO)_9$ core in which one triangular $TeFe_2$ plane was asymmetrically bridged and capped by two bonded Cu atoms at a distance of 2.5988(9) Å (Figure 2). It is noted that the $Cu_2X_2$ fragment in the related complexes $[SeFe_3(CO)_9Cu_2X_2]^{2-}$ (X = Cl, Br) asymmetrically bridged and capped the $Fe_3$ plane.[8] These contrasting bonding modes were probably due to the better overlap between Te and Cu atoms because of the larger size of Te versus Se.

On the other hand, $Cu_3X$-incorporated di-$TeFe_3$ clusters **3b** and **3c** are isostructural species and each consist of two $TeFe_3(CO)_9$ units linked by three Cu atoms in a triangular arrangement where the Cu···Cu bond is externally bridged by one X (X = Br, I) atom, respectively (Figure 4 and Supporting Information, Figure S4). Alternatively, clusters **3b** and **3c** also possess two $TeFe_3$ cores, each with one $TeFe_2$ face capped by a Cu atom, for a $TeFe_3Cu$ trigonal bipyrimidal geometry, two of which are further linked by a $\mu_6$-Cu atom and an X atom (X = Br, I). Noteworthy in **3b** and **3c** is that each Te atom is coordinated to three Fe and two Cu atoms in a $\mu_5$-Te fashion which is rarely cited in the literature.[10] However, in both clusters one of the $\mu_5$-Te atoms possesses the elongated Te−Cu bond, (Te(1)−Cu(1): 3.234(2) Å for **3b**; Te(2)−Cu(3): 2.791(1) Å for **3c**), which is within the van der Waals interaction (the sum of the van der Waals radii for Cu and Te is 3.50 Å; the sum of the covalent radii for Cu and Te is 2.52 Å). Furthermore, three Cu atoms in **3b** and **3c** form an almost isosceles triangle with two short sides and one long side that is further bridged by one X (X = Br, I) atom, giving a $Cu_3X$ bonding mode (Cu(1)−Cu(2): 2.648(2) Å, Cu(2)−Cu(3): 2.777(2) Å, Cu(1)···Cu(3): 3.199(2) Å for **3b**; Cu(1)−Cu(2): 2.681(1) Å, Cu(2)−Cu(3): 2.713(1) Å, Cu(1)···Cu(3): 3.205(2) Å for **3c**). The X-bridged Cu(1)···Cu(3) in **3b** is shorter than that in **3c**, probably because of the smaller size of Br versus I. In addition, the dihedral angles of $Cu_3X$ (X = Br, **3b**; I, **3c**) for **3b** and **3c** are 15.29(7)° and 4.71(4)°, respectively, which indicates that the $Cu_3Br$ ring in **3b** exhibits a butterfly like geometry, but the $Cu_3I$ ring in **3c** displays an almost planar tetragon. It is also noted that clusters **3b** and **3c** represent unprecedented examples of the $Cu_3X$ (X = Br, I) as a bridging unit to coordinate to both main-group and transition-metal atoms. A similar bonding mode of the almost planar $M_3X$ is also found in $[\{Ru_5C(CO)_{14}\}_2Ag_3Cl]^{2-}$.[11]

Further, the $Cu_4Cl_2$-linked di-$TeFe_3$ cluster **4a**, which has a crystallographic center of symmetry at the center of the $Cu_4Cl_2$ hexagonal plane, is shown in Figure 3. The core geometry of **4a** could be described as two $TeFe_3$ units sandwiching a planar $Cu_4Cl_2$ unit. In the $Cu_4Cl_2$ hexagonal plane, the Cl-bridged Cu···Cu distance is 3.849(2) Å, which is significantly longer than the unbridged Cu−Cu edges (2.536(2) Å) because of the effect of the bridging chloride ions and is considered to be nonbonding. The Cl-bridged Cu···Cu distance is longer than the Cl-bridged Cu−Cu edges found in $[\{TeRu_5(CO)_{14}\}_2Cu_4Cl_2]^{2-}$ (2.779(1) Å),[12] $[\{Ru_6C(CO)_{16}\}_2Cu_4Cl_2]^{2-}$ (3.011(4) Å),[13] and $[\{Fe_4Cu_2C(CO)_{12}(\mu\text{-Cl})\}_2]^{2-}$ (2.667(1) Å).[14] Moreover, the bond angle of Cu(1)−Cl(1)−Cu(2a) is 119.4(1)°, which is much larger than that found in $[\{TeRu_5(CO)_{14}\}_2Cu_4Cl_2]^{2-}$ (77.19(5)°),[12] $[\{Ru_6C(CO)_{16}\}_2Cu_4Cl_2]^{2-}$ (86.9(2)°),[13] and $[\{Fe_4Cu_2C(CO)_{12}(\mu\text{-Cl})\}_2]^{2-}$ (92.18(4)°)[14] but closer to $[\{SeFe_3(CO)_9\}_2Cu_4Cl_2]^{2-}$ (104.73(5)°)[8] because of the effect of nonbonded Cu···Cu. The bonding mode of the $M_4X_2$ unit in **4a** is similar to that in $[\{Ru_6C(CO)_{16}\}_2Cu_2Ag_2Cl_2]^{2-}$ and $[\{Ru_6C(CO)_{16}\}_2Ag_4X_2]^{2-}$ (X = Cl, Br, I)[15,16] and is the same as that found in $[\{SeFe_3(CO)_9\}_2Cu_4Cl_2]^{2-}$.[8]

Additionally, it is interesting to note that the Cu atoms in these complexes interact with the C atoms of their neighboring CO ligands that adopt a weakly semibridging geometry. These Cu−C distances are within the van der Waals interaction (2.37(1)−2.58(1) Å, **1a**; 2.429(6)−2.642(9) Å, **1b**; 2.417(8)−2.605(8) Å, **1c**; 2.322(5)−2.866(6) Å, **2a**; 2.24(1)−2.88(1) Å, **3b**; 2.306(8)−2.878(8) Å, **3c**; 2.21(1)−2.894(9) Å, **4a**) and the corresponding Fe−C−O angles are slightly bent from 180° (170.7(9)−177(1)°, **1a**; 173.8(5)−174.9(6)°, **1b**; 173.2(7)−175.4(8)°, **1c**; 167.1(5)−173.6(5)°, **2a**; 166(1)−177(1)°, **3b**; 168.5(7)−175.1(8)°, **3c**; 164.8(9)−176.5(9)°, **4a**) (See Figures 1−4, Supporting Information, Figures S1, S2, and S4).

For comparison, the average bond distances of **1a**−**1c**, **2a**, **3b**, **3c**, **4a**, and related complexes are listed in Table 1. In general, the average Te−Fe, Fe−Fe, Te−Cu, and Fe−Cu distances of **1a**−**1c**, **2a**, **3b**, **3c**, and **4a** were basically similar to those found in the related complexes.[4,5a−5c,9]

(10) (a) Cador, O.; Cattey, H.; Halet, J.-F.; Meier, W.; Mugnier, Y.; Wachter, J.; Saillard, J.-Y.; Zouchoune, B.; Zabel, M. *Inorg. Chem.* **2007**, *46*, 501. (b) Lorenz, A.; Fenske, D. *Angew. Chem., Int. Ed.* **2001**, *40*, 4402. (c) Langetepe, T.; Fenske, D. *Z. Anorg. Allg. Chem.* **2001**, *627*, 820. (d) Eichhöfer, A.; Corrigan, J. F.; Fenske, D.; Tröster, E. *Z. Anorg. Allg. Chem.* **2000**, *626*, 338. (e) Shieh, M.; Chen, H.-S.; Yang, H.-Y.; Ueng, C.-H. *Angew. Chem., Int. Ed.* **1999**, *38*, 1252. (f) Brennan, J. G.; Siegrist, T.; Stuczynski, S. M.; Steigerwald, M. L. *J. Am. Chem. Soc.* **1989**, *111*, 9240. (g) Fenske, D.; Steck, J.-C. *Angew. Chem., Int. Ed. Engl.* **1993**, *32*, 238.

(11) Shephard, D. S.; Maschmeyer, T.; Johnson, B. F. G.; Thomas, J. M.; Sankar, G.; Ozkaya, D.; Zhou, W.; Oldroyd, R. D.; Bell, R. G. *Angew. Chem., Int. Ed. Engl.* **1997**, *36*, 2242.

(12) Shieh, M.; Hsu, M.-H.; Sheu, W.-S.; Jang, L.-F.; Lin, S.-F.; Chu, Y.-Y.; Miu, C.-Y.; Lai, Y.-W.; Liu, H.-L.; Her, J. L. *Chem.—Eur. J.* **2007**, *13*, 6605.

(13) Beswick, M. A.; Lewis, J.; Raithby, P. R.; Ramirez de Arellano, M. C. *J. Chem. Soc., Dalton Trans.* **1996**, 4033.

(14) della Pergola, R.; Sironi, A.; Garlaschelli, L.; Strumolo, D.; Manassero, C.; Manassero, M.; Fedi, S.; Zanello, P.; Kaswalder, F.; Zacchini, S. *Inorg. Chim. Acta* **2009**, DOI: 10.1016/j.ica2009.01.025.

(15) Nakajima, T.; Konomoto, H.; Ogawa, H.; Wakatsuki, Y. *J. Organomet. Chem.* **2007**, *692*, 5071.

(16) Chisholm, D. M.; McIndoe, J. S.; Bodizs, G.; Ang, W. H.; Scopelliti, R.; Dyson, P. J. *J. Cluster Sci.* **2007**, *18*, 303.

**Table 1.** Average Bond Distance (Å) for $[Et_4N]_2[TeFe_3(CO)_9]$, $[Et_4N]_2$[**1a**], $[Et_4N]_2$[**1b**], $[Et_4N]_2$[**1c**], $[Et_4N]_2$[**2a**], $[Et_4N]_2$[**3b**], $[Et_4N]_2$[**3c**], $[Et_4N]_2$[**4a**], and Related Complexes

| complex | Fe−Fe | Te−Fe | Fe−Cu | Te−Cu | Cu−Cu | Cu−X | ref. |
|---|---|---|---|---|---|---|---|
| $[Et_4N]_2[TeFe_3(CO)_9]$ | 2.631(7)[b] | 2.486(9)[b] | | | | | 4 |
| $[Et_4N]_2$[**1a**] | 2.64(1)[b] 2.750(2)[c] | 2.487(6) | 2.48(2) | | | 2.163(3) | a |
| $[Et_4N]_2$[**1b**] | 2.639(3)[b] 2.733(1)[c] | 2.489(4)[b] | 2.49(2) | | | 2.308(1) | a |
| $[Et_4N]_2$[**1c**] | 2.64(1)[b] 2.723(2)[c] | 2.486(8)[b] | 2.48(1) | | | 2.467(1) | a |
| $[Et_4N]_2$[**2a**] | 2.65(2)[b] 2.797(1)[c] | 2.5044(8)[b] 2.518(1)[c] | 2.54(2) | 2.7279(8) | 2.5988(9) | 2.16(1) | a |
| $[Et_4N]_2$[**3b**] | 2.65(1)[b] 2.67(4)[c] | 2.49(1)[b] 2.54(4)[c] | 2.53(3) | 2.8(3) | 2.71(9)[c] 3.199(2)[d] | 2.33(3) | a |
| $[Et_4N]_2$[**3c**] | 2.655(9)[b] 2.68(2)[c] | 2.492(3)[b] 2.56(5)[c] | 2.53(2) | 2.68(8) | 2.70(2)[c] 3.205(2)[d] | 2.50(2) | a |
| $[Et_4N]_2$[**4a**] | 2.74(4)[c] | 2.49(1)[c] | 2.54(2) | | 2.536(2)[c] 3.849(2)[d] | 2.23(6) | a |
| $[PPh_4][TeFe_3(CO)_9(\mu\text{-}AuPPh_3)]$ | 2.621(1)[b] 2.836(3)[c] | 2.49(3)[b] | | | | | 5a |
| [PPN][$HTeFe_3(CO)_9$] | 2.63(1)[b] 2.728(1)[c] | 2.491(3)[b] | | | | | 5b |
| $[H_2TeFe_3(CO)_9]$ | 2.6741(9)[b] 2.70(3)[c] | 2.545(4)[b] | | | | | 5b |
| $[TeFe_3(CO)_9Ir(C_5Me_5)]$ | 2.61(1)[b] 2.585(1)[c] | 2.521(1)[b] 2.53(3)[c] | | | | | 5c |
| $[\{Et_4N\}\{TeFe_3(CO)_9Cu\}]_\infty$ | 2.64(2)[b] | 2.5009(7)[b]2.5269(4)[c] | 2.45(3) | 2.7(1) | | | 9 |
| $[\{TeFe_3(CO)_9Cu_2\}(\mu\text{-}4,4'\text{- dipyridyl})_{1.5}]_\infty$ | 2.634(6)[b] 2.703(3)[c] | 2.505(2)[b] 2.54(4)[c] | 2.52(5) | 2.7(1) | 2.815(2) | | 9 |
| $[TeFe_3(CO)_9Cu_2(MeCN)_2]$ | 2.75(5)[c] | 2.486(3)[b] | 2.52(5) | | | | 9 |
| $[PPh_4]_2[\{TeRu_5(CO)_{14}\}_2Cu_4Cl_2]$ | | | | | 2.608(1)[c] 2.779(1)[d] | 2.23(2) | 12 |
| $[PPN]_2[\{Ru_6Cu_2C(CO)_{16}\}_2Cl_2]$ | | | | | 2.677(3)[c] 3.011(4)[d] | 2.19(1) | 13 |

[a] This work. [b] Unbridged. [c] Bridged by the metal fragment or H. [d] Bridged by the Cl, Br, or I atom.

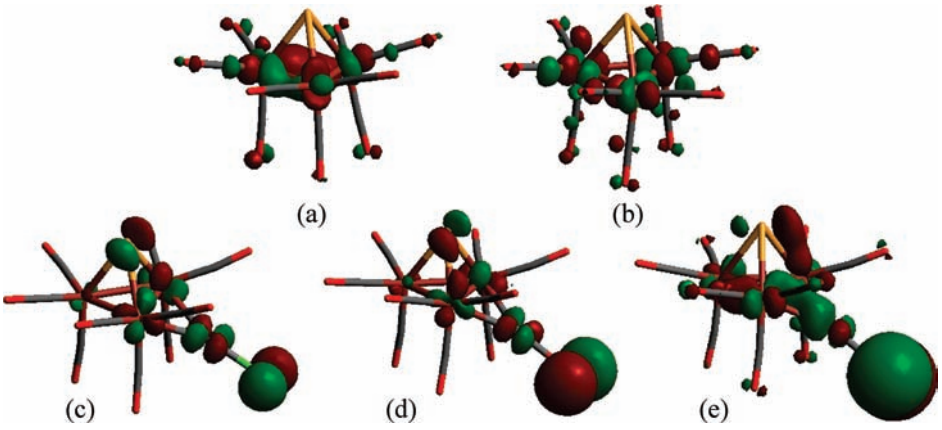


**Figure 5.** Spatial plots of (a) HOMO and (b) LUMO of $[TeFe_3(CO)_9]^{2-}$ and HOMO-3 of (c) **1a**, (d) **1b**, and (e) **1c** (isovalue = 0.032−0.055).

However, the bridged Fe−Fe bond lengths in **1a**−**1c**, **2a**, **3b**, **3c**, and **4a** were significantly longer than their unbridged Fe−Fe distances and the Fe−Fe bond in $[TeFe_3(CO)_9]^{2-}$ because of the effect of bridging copper halide. Similar lengthening of the Te−Fe bonds by the bridging CuCl and the bridging $Cu_3X$ (X = Br, I) units was also noticed in the cases of **2a**, **3b**, and **3c**. The average Te−Cu bond distances for **3b** and **3c** were 2.8(3) and 2.68(8) Å, respectively, which are comparable with that of **2a** (2.7279(8) Å). These unique Te−Cu interactions of the $Cu_2Cl_2$-incorporated $TeFe_3$ complex **2a** and $Cu_3X$-incorporated di-$TeFe_3$ complexes (X = Br, I) **3b** and **3c** were not observed in the CuX-$TeFe_3$ complexes **1a**−**1c** and the $Cu_4Cl_2$-linked di-$TeFe_3$ complex **4a**. Finally, the average Fe−Cu bond distances of **1a**−**1c** (2.48(2), 2.49(2), and 2.48(1) Å) were slightly shorter than those found in **2a** (2.54(2) Å), **3b** (2.53(3) Å), **3c** (2.53(2) Å), and **4a** (2.54(2) Å) probably because of the effect of the size of the metal skeleton.

**DFT Calculations.** To better understand the relevant expansion reactions and the electronic structures of clusters **1a**−**4c**, a hybrid density functional (B3LYP)[17,18] with the modest basis set of LanL2DZ was employed for each complex. The geometry of $[TeFe_3(CO)_9]^{2-}$ was taken from its single-crystal X-ray crystal data and the geometries of **1a**−**1c**, **2a**−**2c**, **2a′**−**2c′**, **3a**−**3c**, and **4a**−**4c** were optimized with the same level of theory.

The calculation shows that the HOMO (highest occupied molecular orbital) of $[TeFe_3(CO)_9]^{2-}$ receives a major contribution from the d orbitals of the Fe atoms (Figure 5a). Thus, it is suggested that CuX (X = Cl, Br, I) could interact with the Fe atoms of $[TeFe_3(CO)_9]^{2-}$ to form Cu−Fe bonds to give clusters **1a**−**1c**. Furthermore, complexes **2a**−**2c** can be seen as the result of the capping of 1 equiv of CuX (X = Cl, Br, I) on the $TeFe_2Cu$ plane of the Fe−Fe bridged CuX-clusters **1a**−**1c**, respectively. The formation of complexes **2a**−**2c** can be related to the HOMO-3 of complexes **1a**−**1c** (Figure 5c−e), each of which receives a significant contribution from the d and p orbitals of the Fe and Cu atoms and from the p orbitals of the Te and X atoms. Further, for the formation of **2a**−**2c** from **1a**−**1c**, the steric effect should also be taken into account. Two orientations of the incoming CuX (X = Cl, Br, I) toward complexes **1a**−**1c** are possible (Scheme 3); one is from the A side (the $TeFe_2Cu$ plane) and the other is from the B side (the $Fe_3Cu$ plane). By considering the larger angle and the less-steric hindrance of the COs for the $TeFe_2Cu$ versus the $Fe_3Cu$ ring, CuX is more susceptible to attack from the A side (forming **2a**−**2c**) rather than from the B side (forming **2a′**−**2c′**). These

(17) (a) Becke, A. D. *J. Chem. Phys.* **1993**, *98*, 5648. (b) Becke, A. D. *J. Chem. Phys.* **1992**, *96*, 2155. (c) Becke, A. D. *J. Chem. Phys.* **1992**, *97*, 9173.
(18) Lee, C.; Yang, W.; Parr, R. G. *Phys. Rev. B* **1988**, *37*, 785.

**Scheme 3**

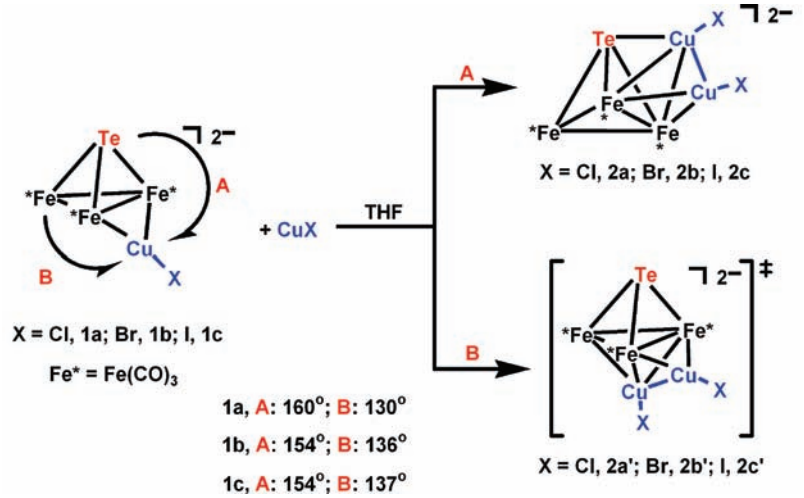


**Scheme 4**

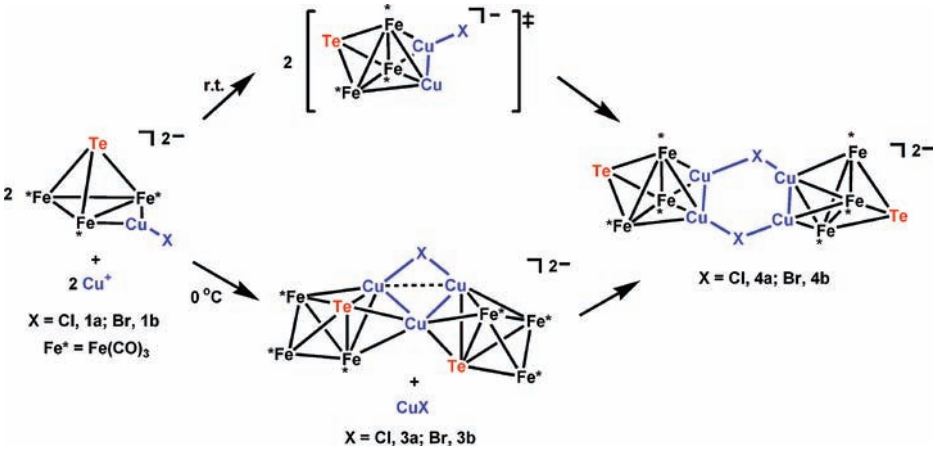


conclusions are supported by the calculations showing complexes **2a**−**2c** to be more stable than the proposed isomers **2a′**−**2c′** ($\Delta E$ = −0.81, −1.38, and −2.05 kcal/mol, respectively).

Moreover, when clusters **1a**−**1c** reacted with $[Cu(MeCN)_4][BF_4]$, clusters **3a**−**3c** were produced. The highest occupied molecular orbital (HOMO) energy levels of **3a**−**3c** were increasingly negative values of **3a** < **3b** < **3c** (−0.04386, −0.04714, and −0.04878 au, respectively) and the HOMO−LUMO energy gaps (LUMO: lowest unoccupied molecular orbital) showed an increasing order of **3a** < **3b** < **3c** (55.56, 57.74, and 58.05 kcal/mol, respectively), which indicated that the stability of **3a**−**3c** was on the order of **3c** > **3b** > **3a**. These results conform to our experimental results that **3a** is less stable than **3b** and **3c** and was not isolated under our conditions.

Furthermore, for complexes **4a**−**4c**, $Cu_4I_2$-linked complex **4c** was not found in our experiments. The HOMO energy levels of **4a**−**4c** show an increasing negative value of **4c** < **4b** < **4a** (−0.09964, −0.10143, and −0.10239 au, respectively), and the HOMO−LUMO energy gaps showed an increasing value of **4c** < **4b** < **4a** (62.53, 63.65, and 64.25 kcal/mol, respectively), indicating that **4c** was the least stable. With the formation of complexes **4a** and **4b** from **1a** and **1b** at room temperature, it was proposed that dicopper-bridged monohalide anionic species "$[TeFe_3(CO)_9Cu_2X]^-$" (X = Cl, Br) could exist as intermediates in the course of the reaction, then undergo a further coupling reaction to produce complexes **4a** and **4b**, respectively (Scheme 4). The calculations showed that the formation of the proposed intermediate $[TeFe_3(CO)_9Cu_2Br]^-$ from complex **1b** was favorable ($\Delta E$ = −454 and $\Delta G$ = −430 kcal/mol) and the reaction energies $\Delta E$ = 6 and $\Delta G$ = 15 kcal/mol were also calculated for a further formation to **4b**, which supported our proposed pathway. On the other hand, the $Cu_3Br$-incorporated complex **3b** was isolated as an intermediate for the formation of **4b** from **1b** at 0 °C, which was also supported by the calculations showing that the formation of complex **3b** from **1b**, and the further transformation of **3b** to **4b**, were both thermally favorable ($\Delta E$ = −403, $\Delta G$ = −379 kcal/mol and $\Delta E$ = −45, $\Delta G$ = −36 kcal/mol, respectively).

The natural population analyses (NPA)[19] and Wiberg bond indices[20] for clusters $[TeFe_3(CO)_9]^{2-}$ and **1a**−**4b** are compared in Table 2. For clusters **1a**−**1c**, **2a**−**2c**, **3b**, **3c**,

(19) (a) Reed, A. E.; Weinhold, F. *J. Chem. Phys.* **1983**, *78*, 4066. (b) Reed, A. E.; Weinstock, R. B.; Weinhold, F. *J. Chem. Phys.* **1985**, *83*, 735.
(20) Wiberg, K. B. *Tetrahedron* **1968**, *24*, 1083.

**Table 2.** Results of Natural Bond Order and Natural Population Analyses of $[TeFe_3(CO)_9]^{2-}$ and Optimized Structures **1a**−**1c**, **2a**−**2c**, **3b**, **3c**, **4a**, and **4b** Calculated at the Level of B3LYP/LanL2DZ

| | Wiberg bond index | | | | | | natural charge | | | | | |
|---|---|---|---|---|---|---|---|---|---|---|---|---|
| complex | Te−Fe | Fe−Fe | Cu−Fe | Cu−X | Cu−Cu | Cu−Te | Te | Fe | Cu | X | $TeFe_3(CO)_9$ (sum) | $Cu_mX_n$ (sum) |
| $[TeFe_3(CO)_9]^{2-}$ ($m = n = 0$) | 0.41 | 0.11 | | | | | −0.19 | −0.41 | | | −2.00 | |
| **1a** ($m = n = 1$) | 0.44 | 0.18 | 0.08 | 0.30 | | | −0.07 | −0.36 | 0.68 | −0.78 | −1.90 | −0.10 |
| **1b** ($m = n = 1$) | 0.44 | 0.20 | 0.08 | 0.30 | | | −0.06 | −0.37 | 0.65 | −0.78 | −1.87 | −0.13 |
| **1c** ($m = n = 1$) | 0.44 | 0.20 | 0.08 | 0.31 | | | −0.06 | −0.36 | 0.64 | −0.77 | −1.87 | −0.13 |
| **2a** ($m = n = 2$) | 0.44 | 0.19 | 0.08 | 0.30 | 0.04 | 0.11 | −0.05 | −0.38 | 0.67 | −0.77 | −1.80 | −0.20 |
| **2b** ($m = n = 2$) | 0.43 | 0.19 | 0.08 | 0.31 | 0.03 | 0.11 | −0.04 | −0.39 | 0.65 | −0.76 | −1.78 | −0.22 |
| **2c** ($m = n = 2$) | 0.43 | 0.19 | 0.07 | 0.33 | 0.03 | 0.11 | −0.05 | −0.37 | 0.63 | −0.75 | −1.76 | −0.24 |
| **3b** ($m = 3, n = 1$) | 0.40 | 0.19 | 0.08 | 0.23 | 0.03 | 0.14 | −0.10 | −0.38 | 0.64 | −0.65 | −3.27 | 1.27 |
| **3c** ($m = 3, n = 1$) | 0.39 | 0.19 | 0.07 | 0.27 | 0.03 | 0.14 | −0.10 | −0.39 | 0.60 | −0.58 | −3.22 | 1.22 |
| **4a** ($m = 4, n = 2$) | 0.46 | 0.18 | 0.09 | 0.18 | 0.05 | | 0.09 | −0.42 | 0.64 | −0.70 | −3.16 | 1.16 |
| **4b** ($m = 4, n = 2$) | 0.45 | 0.18 | 0.09 | 0.21 | 0.05 | | 0.09 | −0.41 | 0.64 | −0.66 | −3.24 | 1.24 |

**4a**, and **4b**, it reveals that the Fe atom carried −0.36 ∼ −0.42 charges while the Cu atom carried +0.60 ∼ +0.68 charges, which suggests some degree of ionic interaction for the Fe−Cu bond. Their relevant Wiberg bond indices ranged from 0.07 to 0.09, which is consistent with the weak bonding between Fe and Cu in these complexes. Further, the sum of the natural charge for $[TeFe_3(CO)_9]^{2-}$ was −2.0, which was more negative than that found in **1a**−**4b**, indicating that the electron density is withdrawn by CuX fragments as CuX (X = Cl, Br, I) was introduced into $[TeFe_3(CO)_9]^{2-}$ (Table 2). The Wiberg bond indices of Cu−X for **1a**−**1c** and **2a**−**2c** ranged from 0.30 to 0.33, which were larger than those found in **3b**, **3c**, **4a**, and **4b** (0.21−0.27), and is indicative of a weaker Cu−X bond as the metal skeleton was increased. In addition, relatively greater Wiberg bond indices were found for the Te−Fe bonds in **1a**−**1c**, **2a**−**2c**, **3b**, **3c**, **4a**, and **4b**, indicating the importance of the Te−Fe bonds for the $TeFe_3$ framework.

**Electrochemistry.** To explore the effect of CuX on the $TeFe_3$ core, we decided to also examine the electrochemical properties of $[Et_4N]_2[TeFe_3(CO)_9]$, $[Et_4N]_2$[**1a**], $[Et_4N]_2$[**1b**], $[Et_4N]_2$[**1c**], $[Et_4N]_2$[**2b**], $[Et_4N]_2$[**3b**], and $[Et_4N]_2$[**4b**] by cyclic voltammetry (CV) and differential pulse voltammetry (DPV). Because of the interference of $Et_4N^+$, the scan range was set between ∼ +0.50 to ∼ −0.10 V and the electrochemical data of all these complexes are summarized in Table 3.

As shown in Figure 6a, the CV of $[TeFe_3(CO)_9]^{2-}$ reveals one quasi-reversible oxidation at $E_{1/2}$ = 0.124 V ($\Delta E$ = 74 mV), one quasi-reversible reduction at $E_{1/2}$ = −0.244 V ($\Delta E$ = 158 mV), and one irreversible reduction wave at −0.523 V. The DPV indicates that these two quasi-reversible, one-electron redox couples appear at 0.135 ($W_{1/2}$ = 105 mV) and −0.270 V ($W_{1/2}$ = 92 mV), respectively (Figure 6b). The DFT calculation shows that the HOMO and LUMO of $[TeFe_3(CO)_9]^{2-}$ came mainly from the $Fe_3$ ring (Figures 5a and 5b), suggesting that the two quasi-reversible reduction and oxidation processes may have occurred in the $Fe_3$ ring.

In the CuX-incorporated system, the electrochemistry of complexes **1a**−**1c**, **2b**, **3b**, and **4b** show some significant differences as compared with that of $[TeFe_3(CO)_9]^{2-}$ (Figure 7 and Supporting Information, Figure S5). As shown in Figure 7a and Supporting Information, Figure S5, the CVs of **1a**−**1c**, **2b**, **3b**, and **4b** are somewhat broad and cannot be assigned unambiguously, but each show a sharp irreversible oxidation peak at around −0.209 to −0.349 V because of the desorption of Cu.[21] Therefore, the DPV studies were further carried out to explore their redox behavior. As listed in Table 3, the DPVs of complexes **1a**−**1c**, **2b**, **3b**, and **4b** each revealed one quasi-reversible oxidation at around 0.236−0.338 V, one quasi-reversible reduction at around −0.116 to −0.162 V, and one irreversible reduction wave at around −0.484 to −0.654 V. It was noted that the quasi-reversible oxidation and the irreversible reduction wave for **1a**−**1c**, **2b**, **3b**, and **4b** were attributable to the $[TeFe_3(CO)_9]^{2-}$ core and the $Cu^+$ ion.[21,22] More importantly, complex **1b** showed a one-electron, quasi-reversible reduction at −0.144 V ($W_{1/2}$ = 132 mV) (Figure 7b), which revealed a more anodic shift (126 mV) compared to that of $[TeFe_3(CO)_9]^{2-}$ (−0.270 V), which was attributed to the presence of the lower electron charge on the $Fe_3$ core owing to the electron-withdrawing effect of the CuBr fragment. Complexes **1a** and **1c** exhibited reduction potentials similar to **1b**, which was indicative of the small effect of halide, which may be understood with the aid of DFT calculations because

**Table 3.** Electrochemical Data of $[Et_4N]_2[TeFe_3(CO)_9]$, $[Et_4N]_2$[**1a**], $[Et_4N]_2$[**1b**], $[Et_4N]_2$[**1c**], $[Et_4N]_2$[**2b**], $[Et_4N]_2$[**3b**], and $[Et_4N]_2$[**4b**]

| | oxidation process | reduction process | |
|---|---|---|---|
| complex | $E^{red}$ (V) | $E^{ox}$ (V) | $E^{red}$ (V) | $E^{red}$ (V) |
| $[Et_4N]_2[TeFe_3(CO)_9]$ | 0.135[a] | | −0.270[a] | −0.523[a] |
| $[Et_4N]_2$[**1a**] | 0.294[a] | −0.289 | −0.146[a] | −0.654[a] |
| $[Et_4N]_2$[**1b**] | 0.256[a] | −0.333 | −0.144[a] | −0.620[a] |
| $[Et_4N]_2$[**1c**] | 0.338[a] | −0.349 | −0.162[a] | −0.618[a] |
| $[Et_4N]_2$[**2b**] | 0.236[a] | −0.259 | −0.124[a] | −0.484[a] |
| $[Et_4N]_2$[**3b**] | 0.292[a] | −0.219 | −0.116[a] | −0.516[a] |
| $[Et_4N]_2$[**4b**] | 0.262[a] | −0.209 | −0.130[a] | −0.486[a] |

[a] From differential pulse voltammetry.

(21) (a) Xue, X.; Wang, X.-S.; Xiong, R.-G.; You, X.-Z.; Abrahams, B. F.; Che, C.-M.; Ju, H.-X. *Angew. Chem., Int. Ed.* **2002**, *41*, 2944. (b) Scheer, M.; Schindler, A.; Merkle, R.; Johnson, B. P.; Linseis, M.; Winter, R.; Anson, C. E.; Virovets, A. V. *J. Am. Chem. Soc.* **2007**, *129*, 13386. (c) Doescher, M. S.; Tour, J. M.; Rawlett, A. M.; Myrick, M. L. *J. Phys. Chem. B* **2001**, *105*, 105. (d) Hagenström, H.; Schneeweiss, M. A.; Kolb, D. M. *Langmuir* **1999**, *15*, 7802.

(22) (a) Yam, V. W.-W.; Lee, W.-K.; Lai, T.-F. *Organometallics* **1993**, *12*, 2383. (b) Yam, V. W.-W.; Lee, W.-K.; Cheung, K.-K.; Crystall, B.; Phillips, D. *J. Chem. Soc., Dalton Trans.* **1996**, 3283. (c) Yam, V. W.-W.; Fung, W. K.-M.; Wong, M.-T. *Organometallics* **1997**, *16*, 1772. (d) Yam, V. W.-W.; Fung, W. K.-M.; Cheung, K.-K. *Organometallics* **1998**, *17*, 3293.

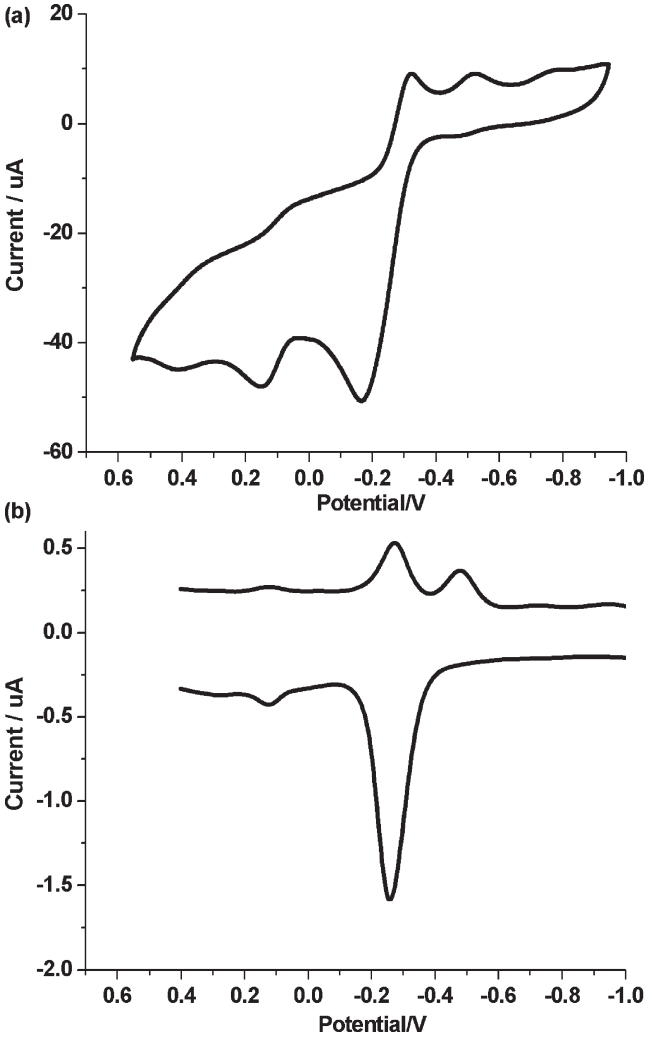


**Figure 6.** (a) Cyclic voltammogram (CV) and (b) differential pulse voltammogram (DPV) in $CH_3CN$ solution for $[Et_4N]_2[TeFe_3(CO)_9]$ ($10^{-3}$ M). Conditions: electrolyte, 0.1 M $Bu_4NClO_4$; working electrode, platinum electrode; scan rate, 100 mV $s^{-1}$. Potential are vs SCE.

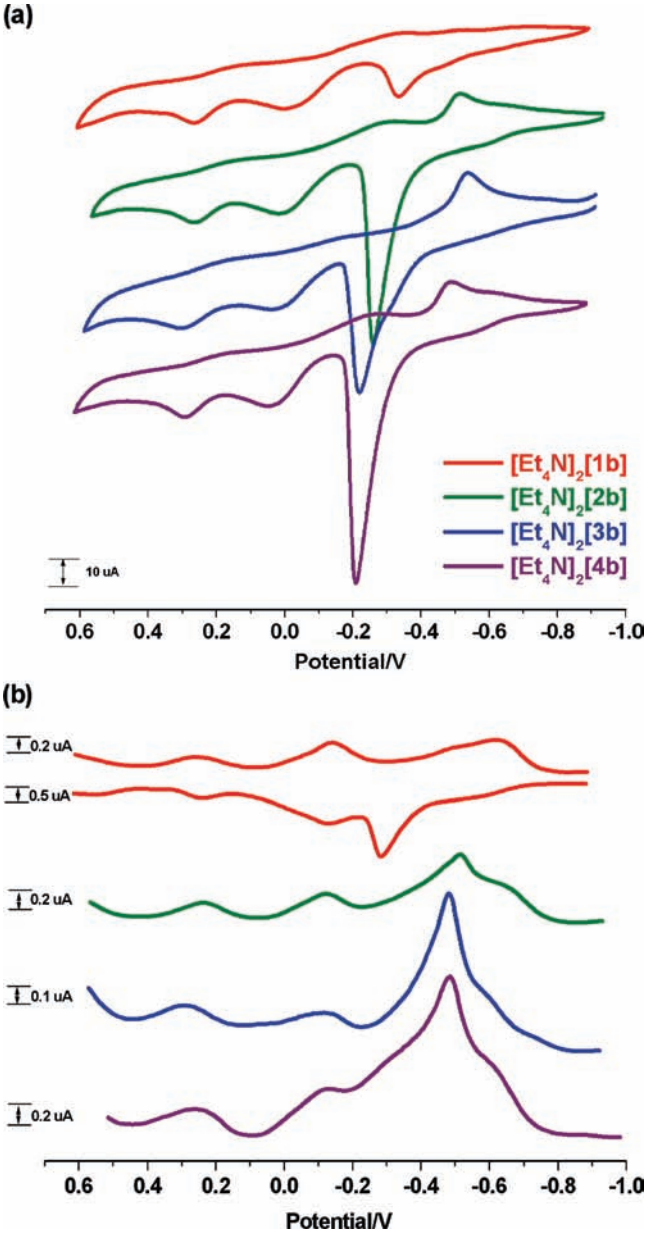


**Figure 7.** (a) Cyclic voltammograms (CVs) and (b) differential pulse voltammograms (DPVs) in $CH_3CN$ solution for $[Et_4N]_2$[**1b**], $[Et_4N]_2$[**2b**], $[Et_4N]_2$[**3b**], and $[Et_4N]_2$[**4b**] with a concentration of $10^{-3}$ M. Conditions: electrolyte, 0.1 M $Bu_4NClO_4$; working electrode, platinum electrode; scan rate, 100 mV $s^{-1}$. Potential are vs SCE.

of the close values for their electron affinity and the LUMO energy level (Supporting Information, Table S1).

In addition, compared with the one-electron reduction at −0.144 V for **1b**, complexes **2b**, **3b**, and **4b** each showed a quasi-reversible reduction at −0.124, −0.116, and −0.130 V, respectively (Table 3 and Figure 7b), approximately consistent with the decreasing negative charges for each $TeFe_3(CO)_9$ core from **1b**, **2b**, to **3b** (Table 2), which was related to the increased size of the skeleton and the higher number of CuBr or $Cu^+$ incorporated into the $TeFe_3(CO)_9$ core. The exception in the case of **4b** may be related to the fact that the LUMO of **4b** had the least percentage of contribution from the $TeFe_3$ core compared with those of **1b**−**3b**. Lastly, the decreased negative quasi-reversible reduction potentials for **2b**, **3b**, and **4b** versus **1b** can be explained by the calculated electron affinity and the LUMO energy level (Supporting Information, Table S1).

## Conclusion

A new series of nanosized CuX-, $Cu_2X_2$-, $Cu_3X$-, and $Cu_4X_2$-incorporated mono- or di-$TeFe_3$-based complexes were systematically synthesized from the reactions of $[TeFe_3(CO)_9]^{2-}$ with appropriate amounts of CuX or followed by $[Cu(MeCN)_4][BF_4]$. The effect of CuX or $Cu^+$ on the stepwise cluster growth processes and their electrochemistry were investigated in detail with respect to the coupling effect of the $TeFe_3$ core and the size of the metal skeleton, which is supported by theoretical calculations. Some significant characteristics were noted. First, novel $Cu_3X$-incorporated di-$TeFe_3$ clusters $[\{TeFe_3(CO)_9\}_2Cu_3X]^{2-}$ (X = Cl, Br) are kinetically controlled intermediates for the formation of $Cu_4X_2$-linked di-$TeFe_3$ clusters, which represent unprecedented examples of $Cu_3X$ (X = Br, I) as the bridging units that coordinate to both main-group and transition-metal atoms. Second, pronounced anodic shifts for the electrochemical reduction of the $TeFe_3$ core were noticed as an

increased number of either CuX or $Cu^+$ were introduced or as the size of the metal skeleton was increased. Lastly, this study provides a thorough review of the construction of ternary Te−Fe−Cu clusters from both synthetic and theoretical viewpoints.

## Experimental Section

All reactions were performed under an atmosphere of pure nitrogen using standard Schlenk techniques.[23] Solvents were purified, dried, and distilled under nitrogen prior to use. CuCl (Aldrich), CuBr (Strem), and CuI (Aldrich) were used as received. $[Et_4N]_2[TeFe_3(CO)_9]$[6d] and $[Cu(MeCN)_4][BF_4]$[24] were prepared according to the published methods. Infrared spectra were recorded on a Perkin-Elmer Paragon 500 IR spectrometer as solutions in $CaF_2$ cells. Elemental analyses of C, H, and N were performed on a Perkin-Elmer 2400 analyzer at the NSC Regional Instrumental Center at National Taiwan University, Taipei, Taiwan.

**Synthesis of $[Et_4N]_2[TeFe_3(CO)_9CuCl]$ ($[Et_4N]_2$[1a]).** THF (20 mL) was added to a mixture of 0.50 g (0.62 mmol) of $[Et_4N]_2[TeFe_3(CO)_9]$ and 0.067 g (0.68 mmol) of CuCl in an ice−water bath. The mixture was stirred in an ice−water bath for 15 min to give a reddish-brown solution, which was filtered, and solvent was removed under vacuum. The residue was then washed with $Et_2O$/MeOH several times and extracted with THF, which was recrystallized with $Et_2O$/MeOH/THF to give 0.44 g (0.49 mmol) of the reddish-brown sample of $[Et_4N]_2[TeFe_3(CO)_9CuCl]$ ($[Et_4N]_2$[**1a**]) (79% based on $[Et_4N]_2[TeFe_3(CO)_9]$). IR ($\nu_{CO}$, THF): 2008 (w), 1947 (vs), 1919 (m), 1890 (w), 1862 (w) $cm^{-1}$. Anal. Calcd for $[Et_4N]_2$[**1a**]: C, 33.12; H, 4.45; N, 3.09. Found: C, 33.21; H, 4.43; N, 2.97. Crystals of $[Et_4N]_2$[**1a**] suitable for single-crystal X-ray analysis were grown from $Et_2O$/THF.

**Synthesis of $[Et_4N]_2[TeFe_3(CO)_9CuBr]$ ($[Et_4N]_2$[1b]).** The preparation and purification of $[Et_4N]_2$[**1b**] was similar to that of $[Et_4N]_2$[**1a**] by using 0.50 g (0.62 mmol) of $[Et_4N]_2[TeFe_3(CO)_9]$ and 0.099 g (0.69 mmol) of CuBr. The yield was 0.42 g (0.44 mmol) of $[Et_4N]_2[TeFe_3(CO)_9CuBr]$ ($[Et_4N]_2$[**1b**]) (71% based on $[Et_4N]_2[TeFe_3(CO)_9]$). IR ($\nu_{CO}$, THF): 2008 (w), 1947 (vs), 1918 (m), 1890 (w), 1863 (w) $cm^{-1}$. Anal. Calcd for $[Et_4N]_2$[**1b**]: C, 31.52; H, 4.24; N, 2.94. Found: C, 31.56; H, 4.40; N, 2.97. Crystals of $[Et_4N]_2$[**1b**] suitable for single-crystal X-ray analysis were grown from $Et_2O$/MeOH/THF.

**Synthesis of $[Et_4N]_2[TeFe_3(CO)_9CuI]$ ($[Et_4N]_2$[1c]).** The preparation and purification of $[Et_4N]_2$[**1c**] was similar to that of $[Et_4N]_2$[**1a**] by using 0.50 g (0.62 mmol) of $[Et_4N]_2[TeFe_3(CO)_9]$ and 0.13 g (0.68 mmol) of CuI. The yield was 0.59 g (0.59 mmol) of $[Et_4N]_2[TeFe_3(CO)_9CuI]$ ($[Et_4N]_2$[**1c**]) (95% based on $[Et_4N]_2[TeFe_3(CO)_9]$). IR ($\nu_{CO}$, THF): 2008 (w), 1948 (vs), 1918 (m), 1892 (w), 1865 (w), 1780 (w) $cm^{-1}$. Anal. Calcd for $[Et_4N]_2$[**1c**]: C, 30.01; H, 4.03; N, 2.80. Found: C, 30.01; H, 4.14; N, 2.66. Crystals of $[Et_4N]_2$[**1c**] suitable for single-crystal X-ray analysis were grown from $Et_2O$/MeOH/THF.

**Synthesis of $[Et_4N]_2[TeFe_3(CO)_9Cu_2Cl_2]$ ($[Et_4N]_2$[2a]).** THF (20 mL) was added to a mixture of 0.50 g (0.62 mmol) of $[Et_4N]_2[TeFe_3(CO)_9]$ and 0.14 g (1.41 mmol) of CuCl in an ice−water bath. The mixture was stirred in an ice−water bath for 3.5 h to give a purple solution, which was filtered, and solvent was removed under vacuum. The residue was then washed with $Et_2O$ several times and extracted with THF, which was recrystallized with $Et_2O$/THF to give 0.40 g (0.40 mmol) of $[Et_4N]_2[TeFe_3(CO)_9Cu_2Cl_2]$ ($[Et_4N]_2$[**2a**]) (65% based on $[Et_4N]_2[TeFe_3(CO)_9]$). IR ($\nu_{CO}$, THF): 2019 (m), 1972 (s,br), 1910 (w) $cm^{-1}$. Anal. Calcd for $[Et_4N]_2$[**2a**]: C, 29.83; H, 4.01; N, 2.78. Found: C, 29.68; H, 4.21; N, 2.78. Crystals of $[Et_4N]_2$[**2a**] suitable for single-crystal X-ray analysis were grown from $Et_2O$/THF.

**Synthesis of $[Et_4N]_2[TeFe_3(CO)_9Cu_2Br_2]$ ($[Et_4N]_2$[2b]).** The preparation and purification of $[Et_4N]_2$[**2b**] was similar to that of $[Et_4N]_2$[**2a**] by using 0.50 g (0.62 mmol) of $[Et_4N]_2[TeFe_3(CO)_9]$ and 0.22 g (1.53 mmol) of CuBr. The yield was 0.56 g (0.51 mmol) of $[Et_4N]_2[TeFe_3(CO)_9Cu_2Br_2]$ ($[Et_4N]_2$[**2b**]) (82% based on $[Et_4N]_2[TeFe_3(CO)_9]$). IR ($\nu_{CO}$, THF): 2019 (m), 1973 (s,br), 1961 (m,sh), 1898 (w) $cm^{-1}$. Anal. Calcd for $[Et_4N]_2$[**2b**]: C, 27.43; H, 3.69; N, 2.56. Found: C, 27.55; H, 3.67; N, 2.54.

**Synthesis of $[Et_4N]_2[TeFe_3(CO)_9Cu_2I_2]$ ($[Et_4N]_2$[2c]).** MeCN (20 mL) was added to a mixture of 0.40 g (0.50 mmol) of $[Et_4N]_2[TeFe_3(CO)_9]$ and 0.29 g (1.52 mmol) of CuI in an ice−water bath. The mixture was stirred in an ice−water bath for 20 h to give a reddish-brown solution, which was filtered, and solvent was removed under vacuum. The residue was then washed with hexanes and $Et_2O$ several times. The THF extract was recrystallized with $Et_2O$/THF to give 0.30 g (0.25 mmol) of a reddish-brown sample of $[Et_4N]_2[TeFe_3(CO)_9Cu_2I_2]$ ($[Et_4N]_2$[**2c**]) (50% based on $[Et_4N]_2[TeFe_3(CO)_9]$). IR ($\nu_{CO}$, THF): 2019 (m), 1973 (s,br), 1961 (m,sh), 1895 (w) $cm^{-1}$. Anal. Calcd for $[Et_4N]_2$[**2c**]: C, 25.22; H, 3.39; N, 2.35. Found: C, 25.55; H, 3.07; N, 2.06.

**Synthesis of $[Et_4N]_2[\{TeFe_3(CO)_9\}_2Cu_3Cl]$ ($[Et_4N]_2$[3a]).** THF (15 mL) was added to a mixture of 0.19 g (0.21 mmol) of $[Et_4N]_2$[**1a**] and 0.070 g (0.22 mmol) of $[Cu(MeCN)_4][BF_4]$ in an ice−water bath. The mixture was stirred in an ice−water bath for 30 min to give a purplish-brown solution, which was filtered, and solvent was removed under vacuum. The residue was then washed with $Et_2O$ several times. The THF extract solution was shown by IR spectroscopy to be $[Et_4N]_2[\{TeFe_3(CO)_9\}_2Cu_3Cl]$ ($[Et_4N]_2$[**3a**]) by comparison with those of $[Et_4N]_2$[**3b**] and $[Et_4N]_2$[**3c**]. IR ($\nu_{CO}$, THF): 2018 (vw), 1972 (s), 1959 (vs), 1902 (w) $cm^{-1}$.

**Synthesis of $[Et_4N]_2[\{TeFe_3(CO)_9\}_2Cu_3Br]$ ($[Et_4N]_2$[3b]).** THF (15 mL) was added to a mixture of 0.15 g (0.16 mmol) of $[Et_4N]_2$[**1b**] and 0.051 g (0.16 mmol) of $[Cu(MeCN)_4][BF_4]$ in an ice−water bath. The mixture was stirred in an ice−water bath for 30 min to give a purplish-brown solution, which was filtered, and solvent was removed under vacuum. The residue was then washed with $Et_2O$ several times. The THF extract was recrystallized with $Et_2O$/THF to give 0.11 g (0.07 mmol) of a purplish-brown sample of $[Et_4N]_2[\{TeFe_3(CO)_9\}_2Cu_3Br]$ ($[Et_4N]_2$[**3b**]) (88% based on $[Et_4N]_2$[**1b**]). IR ($\nu_{CO}$, THF): 2019 (m), 1972 (s), 1959 (vs), 1903 (w) $cm^{-1}$. Anal. Calcd for $[Et_4N]_2$[**3b**]: C, 25.07; H, 2.48; N, 1.72. Found: C, 25.34; H, 2.69; N, 1.50. Crystals of $[Et_4N]_2$[**3b**] suitable for single-crystal X-ray analysis were grown from $Et_2O$/THF.

**Synthesis of $[Et_4N]_2[\{TeFe_3(CO)_9\}_2Cu_3I]$ ($[Et_4N]_2$[3c]).** The preparation and purification of $[Et_4N]_2$[**3c**] was similar to that of $[Et_4N]_2$[**3b**] by using 0.18 g (0.18 mmol) of $[Et_4N]_2$[**1c**] and 0.067 g (0.21 mmol) of $[Cu(MeCN)_4][BF_4]$. The yield was 0.10 g (0.06 mmol) of $[Et_4N]_2[\{TeFe_3(CO)_9\}_2Cu_3I]$ ($[Et_4N]_2$[**3c**]) (67% based on $[Et_4N]_2$[**1c**]). IR ($\nu_{CO}$, THF): 2018 (m), 1975 (s), 1957 (vs), 1893 (w) $cm^{-1}$. Anal. Calcd for $[Et_4N]_2$[**3c**]: C, 24.35; H, 2.41; N, 1.67. Found: C, 24.46; H, 2.47; N, 1.58. Crystals of $[Et_4N]_2$[**3c**] suitable for single-crystal X-ray analysis were grown from $Et_2O$/THF.

**Synthesis of $[Et_4N]_2[\{TeFe_3(CO)_9\}_2Cu_4Cl_2]$ ($[Et_4N]_2$[4a]).** THF (20 mL) was added to a mixture of 0.50 g (0.62 mmol) of $[Et_4N]_2[TeFe_3(CO)_9]$ and 0.27 g (2.73 mmol) of CuCl in an ice−water bath. The mixture was stirred at room temperature for 4 h to give a purplish-brown solution, which was filtered, and solvent was removed under vacuum. The residue was then washed with hexanes and $Et_2O$ several times. The THF extract

(23) Shriver, D. F.; Drezdon, M. A. *The Manipulation of Air-Sensitive Compounds*; Wiley-VCH Publishers: New York, 1986.

(24) (a) Kubas, G. J. *Inorg. Synth.* **1979**, *19*, 90. (b) Simmons, M. G.; Merrill, C. L.; Wilson, L. J.; Bottomley, L. A.; Kadish, K. M. *J. Chem. Soc., Dalton Trans.* **1980**, 1827.

was recrystallized with $Et_2O$/THF to give 0.36 g (0.21 mmol) of a purplish-brown sample of $[Et_4N]_2[\{TeFe_3(CO)_9\}_2Cu_4Cl_2]$ ($[Et_4N]_2$[**4a**]) (68% based on $[Et_4N]_2[TeFe_3(CO)_9]$). IR ($\nu_{CO}$, THF): 2019 (vw), 1982 (vs), 1970 (s), 1934 (vw), 1911 (w) $cm^{-1}$. Anal. Calcd for $[Et_4N]_2$[**4a**]: C, 24.31; H, 2.40; N, 1.67. Found: C, 24.07; H, 2.38; N, 1.84. Crystals of $[Et_4N]_2$[**4a**] suitable for single-crystal X-ray analysis were grown from $Et_2O$/THF.

**Synthesis of $[Et_4N]_2[\{TeFe_3(CO)_9\}_2Cu_4Br_2]$ ($[Et_4N]_2$[4b]).** The preparation and purification of $[Et_4N]_2$[**4b**] was similar to that of $[Et_4N]_2$[**4a**] by using 0.50 g (0.62 mmol) of $[Et_4N]_2[TeFe_3(CO)_9]$ and 0.36 g (2.51 mmol) of CuBr. The yield was 0.48 g (0.27 mmol) of $[Et_4N]_2[\{TeFe_3(CO)_9\}_2Cu_4Br_2]$ ($[Et_4N]_2$[**4b**]) (87% based on $[Et_4N]_2[TeFe_3(CO)_9]$). IR ($\nu_{CO}$, THF): 2019 (w), 1982 (vs), 1970 (s), 1936 (vw), 1910 (w) $cm^{-1}$. Anal. Calcd for $[Et_4N]_2$[**4b**]: C, 23.09; H, 2.28; N, 1.58. Found: C, 22.84; H, 2.24; N, 1.37.

**Conversion of $[Et_4N]_2$[1a] to $[Et_4N]_2$[2a].** THF (15 mL) was added to a mixture of 0.18 g (0.20 mmol) of $[Et_4N]_2$[**1a**] and 0.022 g (0.22 mmol) of CuCl in an ice−water bath. The mixture was stirred in an ice−water bath for 30 min to give a reddish-brown solution, which was filtered, and solvent was removed under vacuum. The residue was then washed with hexanes and $Et_2O$ several times. The THF extract was recrystallized with $Et_2O$/THF to give 0.14 g (0.14 mmol) of $[Et_4N]_2$[**2a**] (70% based on $[Et_4N]_2$[**1a**]).

**Conversion of $[Et_4N]_2$[1b] to $[Et_4N]_2$[2b].** Similar to the conversion of $[Et_4N]_2$[**1a**] to $[Et_4N]_2$[**2a**], the reaction was carried out by using 0.18 g (0.19 mmol) of $[Et_4N]_2$[**1b**] and 0.031 g (0.22 mmol) of CuBr. The yield was 0.11 g (0.10 mmol) of $[Et_4N]_2$[**2b**] (53% based on $[Et_4N]_2$[**1b**]).

**Conversion of $[Et_4N]_2$[1c] to $[Et_4N]_2$[2c].** MeCN (20 mL) was added to a mixture of 0.62 g (0.62 mmol) of $[Et_4N]_2$[**1c**] and 0.24 g (1.26 mmol) of CuI in an ice−water bath. The mixture was stirred in an ice−water bath for 24 h to give a reddish-brown solution, which was filtered, and solvent was removed under vacuum. The residue was then washed with hexanes and $Et_2O$ several times. The THF extract was recrystallized with $Et_2O$/THF to give 0.51 g (0.43 mmol) of $[Et_4N]_2$[**2c**] (69% based on $[Et_4N]_2$[**1c**]).

**Conversion of $[Et_4N]_2$[2a] to $[Et_4N]_2$[4a].** THF (10 mL) was added to a mixture of 0.06 g (0.06 mmol) of $[Et_4N]_2$[**2a**] and 0.020 g (0.06 mmol) of $[Cu(MeCN)_4][BF_4]$ in an ice−water bath. The mixture was stirred at room temperature for 2 h to give a purplish solution, which was filtered, and solvent was removed under vacuum. The residue was then washed with hexanes and $Et_2O$ several times. The THF extract was recrystallized with $Et_2O$/THF to give 0.04 g (0.02 mmol) of $[Et_4N]_2$[**4a**] (67% based on $[Et_4N]_2$[**2a**]).

**Conversion of $[Et_4N]_2$[2b] to $[Et_4N]_2$[4b].** Similar to the conversion of $[Et_4N]_2$[**2a**] to $[Et_4N]_2$[**4a**], the reaction was carried out by using 0.22 g (0.20 mmol) of $[Et_4N]_2$[**2b**] and 0.063 g (0.20 mmol) of $[Cu(MeCN)_4][BF_4]$. The yield was 0.16 g (0.09 mmol) of $[Et_4N]_2$[**4b**] (90% based on $[Et_4N]_2$[**2b**]).

**Conversion of $[Et_4N]_2$[2c] to $[Et_4N]_2$[3c].** THF (20 mL) was added to a mixture of 0.30 g (0.25 mmol) of $[Et_4N]_2$[**2c**] and 0.080 g (0.25 mmol) of $[Cu(MeCN)_4][BF_4]$ in an ice−water bath. The mixture was stirred at room temperature for 5 h to give a brown solution, which was filtered, and solvent was removed under vacuum. The residue was then washed with hexanes and $Et_2O$ several times. The THF extract was recrystallized with $Et_2O$/THF to give 0.17 g (0.10 mmol) of $[Et_4N]_2$[**3c**] (80% based on $[Et_4N]_2$[**2c**]).

**Conversion of $[Et_4N]_2$[3b] to $[Et_4N]_2$[4b].** THF (15 mL) was added to a mixture of 0.16 g (0.10 mmol) of $[Et_4N]_2$[**3b**] and 0.015 g (0.10 mmol) of CuBr in an ice−water bath. The mixture was stirred at room temperature for 4 h to give a purplish solution, which was filtered, and solvent was removed under vacuum. The residue was then washed with hexanes and $Et_2O$ several times. The THF extract was recrystallized with $Et_2O$/THF to give 0.12 g (0.07 mmol) of $[Et_4N]_2$[**4b**] (70% based on $[Et_4N]_2$[**3b**]).

**Conversion of $[Et_4N]_2$[1a] to $[Et_4N]_2$[4a].** THF (20 mL) was added to a mixture of 0.23 g (0.25 mmol) of $[Et_4N]_2$[**1a**] and 0.081 g (0.26 mmol) of $[Cu(MeCN)_4][BF_4]$ in an ice−water bath. The mixture was stirred at room temperature for 4.5 h to give a purplish solution, which was filtered, and solvent was removed under vacuum. The residue was then washed with hexanes and $Et_2O$ several times and extracted with THF to give 0.18 g (0.11 mmol) of $[Et_4N]_2$[**4a**] (88% based on $[Et_4N]_2$[**1a**]).

**Conversion of $[Et_4N]_2$[1b] to $[Et_4N]_2$[4b].** Similar to the conversion of $[Et_4N]_2$[**1a**] to $[Et_4N]_2$[**4a**], the reaction was carried out by using 0.19 g (0.20 mmol) of $[Et_4N]_2$[**1b**] and 0.063 g (0.20 mmol) of $[Cu(MeCN)_4][BF_4]$. The yield was 0.11 g (0.06 mmol) of $[Et_4N]_2$[**4b**] (60% based on $[Et_4N]_2$[**1b**]).

**X-ray Structural Characterization of $[Et_4N]_2[TeFe_3(CO)_9CuCl]$ ($[Et_4N]_2$[1a]), $[Et_4N]_2[TeFe_3(CO)_9CuBr]$ ($[Et_4N]_2$[1b]),** $[Et_4N]_2[TeFe_3(CO)_9CuI]$ ($[Et_4N]_2$[1c]), $[Et_4N]_2[TeFe_3(CO)_9Cu_2Cl_2]$ ($[Et_4N]_2$[2a]), $[Et_4N]_2[\{TeFe_3(CO)_9\}_2Cu_3Br]$ ($[Et_4N]_2$[3b]), $[Et_4N]_2[\{TeFe_3(CO)_9\}_2Cu_3I]$ ($[Et_4N]_2$[3c]), and $[Et_4N]_2[\{TeFe_3(CO)_9\}_2Cu_4Cl_2]$ ($[Et_4N]_2$[4a]). Selected crystallographic data for $[Et_4N]_2$[**1a**], $[Et_4N]_2$[**1b**], $[Et_4N]_2$[**1c**], $[Et_4N]_2$[**2a**], $[Et_4N]_2$[**3b**], $[Et_4N]_2$[**3c**], and $[Et_4N]_2$[**4a**] are given in Table 4. Selected bond distances and angles of $[Et_4N]_2$[**1a**], $[Et_4N]_2$[**1b**], $[Et_4N]_2$[**1c**], $[Et_4N]_2$[**2a**], $[Et_4N]_2$[**3b**], $[Et_4N]_2$[**3c**], and $[Et_4N]_2$[**4a**] are shown in Supporting Information, Table S2. All crystals were mounted on glass fibers with epoxy cement. Data collection for $[Et_4N]_2$[**1a**] was carried out using a Siemens Smart CCD (charged coupled device) diffractometer. Data collection for $[Et_4N]_2$[**1b**], $[Et_4N]_2$[**1c**], $[Et_4N]_2$[**2a**], $[Et_4N]_2$[**3b**], $[Et_4N]_2$[**3c**], and $[Et_4N]_2$[**4a**] was carried out using a Bruker-Nonius Kappa CCD diffractometer with graphite-monochromated $Mo_{K\alpha}$ radiation in the $2\theta$ range of 2.0−50°, and an empirical absorption correction by multiscan was applied.[25] The structures of $[Et_4N]_2$[**1a**]−$[Et_4N]_2$[**4a**] were refined by SHELXL packages,[26] and all of the non-hydrogen atoms were refined with anisotropic temperature factors.

**Computational Details.** All calculations reported in this study were performed via the DFT[27] with Becke's three-parameter (B3) exchange functional and the Lee−Yang−Parr (LYP) correlation functional (B3LYP)[17,18] with a LanL2DZ basis set using the Gaussian 03 series of packages. The geometry of $[TeFe_3(CO)_9]^{2-}$ was taken from its single-crystal X-ray crystal data without further modification. The geometries of **1a**−**1c**, **2a**−**2c**, **2a′**−**2c′**, **3a**−**3c**, and **4a**−**4c** were optimized and found to be local minima in a potential energy surface by performing frequency calculations and by observing a lack of imaginary vibrations. Natural charges[19] and Wiberg bond indices[20] were evaluated using the Weinhold NBO method.[28] Graphical

(25) Blessing, R. H. *Acta Crystallogr., Sect. A* **1995**, *51*, 33.
(26) Sheldrick, G. M. *SHELXL97*, version 97−2; University of Göttingen: Göttingen, Germany, 1997.
(27) Frisch, M. J.; Trucks, G. W.; Schlegel, H. B.; Scuseria, G. E.; Robb, M. A.; Cheeseman, J. R.; Montgomery, Jr., J. A.; Vreven, T.; Kudin, K. N.; Burant, J. C.; Millam, J. M.; Iyengar, S. S.; Tomasi, J.; Barone, V.; Mennucci, B.; Cossi, M.; Scalmani, G.; Rega, N.; Petersson, G. A.; Nakatsuji, H.; Hada, M.; Ehara, M.; Toyota, K.; Fukuda, R.; Hasegawa, J.; Ishida, M.; Nakajima, T.; Honda, Y.; Kitao, O.; Nakai, H.; Klene, M.; Li, X.; Knox, J. E.; Hratchian, H. P.; Cross, J. B.; Bakken, V.; Adamo, C.; Jaramillo, J.; Gomperts, R.; Stratmann, R. E.; Yazyev, O.; Austin, A. J.; Cammi, R.; Pomelli, C.; Ochterski, J. W.; Ayala, P. Y.; Morokuma, K.; Voth, G. A.; Salvador, P.; Dannenberg, J. J.; Zakrzewski, V. G.; Dapprich, S.; Daniels, A. D.; Strain, M. C.; Farkas, O.; Malick, D. K.; Rabuck, A. D.; Raghavachari, K.; Foresman, J. B.; Ortiz, J. V.; Cui, Q.; Baboul, A. G.; Clifford, S.; Cioslowski, J.; Stefanov, B. B.; Liu, G.; Liashenko, A.; Piskorz, P.; Komaromi, I.; Martin, R. L.; Fox, D. J.; Keith, T.; Al-Laham, M. A.; Peng, C. Y.; Nanayakkara, A.; Challacombe, M.; Gill, P. M. W.; Johnson, B.; Chen, W.; Wong, M. W.; Gonzalez, C.; Pople, J. A. *Gaussian 03*, Revision B.04; Gaussian, Inc.: Wallingford, CT, 2004.
(28) Reed, A. E.; Curtiss, L. A.; Weinhold, F. *Chem. Rev.* **1988**, *88*, 899.

**Table 4.** Crystallographic Data for $[Et_4N]_2[TeFe_3(CO)_9CuCl]$ ($[Et_4N]_2$[**1a**]), $[Et_4N]_2[TeFe_3(CO)_9CuBr]$ ($[Et_4N]_2$[**1b**]), $[Et_4N]_2[TeFe_3(CO)_9CuI]$ ($[Et_4N]_2$[**1c**]) $[Et_4N]_2[TeFe_3(CO)_9Cu_2Cl_2]$ ($[Et_4N]_2$[**2a**]), $[Et_4N]_2[\{TeFe_3(CO)_9\}_2Cu_3Br]$ ($[Et_4N]_2$[**3b**]), $[Et_4N]_2[\{TeFe_3(CO)_9\}_2Cu_3I]$ ($[Et_4N]_2$[**3c**]), and $[Et_4N]_2[\{TeFe_3(CO)_9\}_2Cu_4Cl_2]$ ($[Et_4N]_2$[**4a**])

| | $[Et_4N]_2$[**1a**] | $[Et_4N]_2$[**1b**] | $[Et_4N]_2$[**1c**] |
|---|---|---|---|
| empirical formula | $C_{25}H_{40}ClCuFe_3N_2O_9Te$ | $C_{25}H_{40}BrCuFe_3N_2O_9Te$ | $C_{25}H_{40}ICuFe_3N_2O_9Te$ |
| formula weight | 906.73 | 951.19 | 998.18 |
| crystal system | monoclinic | triclinic | triclinic |
| space group | $C_C$ | $P\bar{1}$ | $P\bar{1}$ |
| crystal dimensions, mm | 0.22 × 0.20 × 0.18 | 0.38 × 0.18 × 0.11 | 0.38 × 0.24 × 0.06 |
| $a$, Å | 18.953(3) | 9.0411(1) | 9.4787(2) |
| $b$, Å | 12.944(2) | 20.2015(3) | 10.2155(2) |
| $c$, Å | 29.403(5) | 21.3876(4) | 19.0383(4) |
| α, deg | | 65.656(1) | 82.241(1) |
| $\beta$, deg | 99.278(4) | 89.869(1) | 79.680(1) |
| $\gamma$, deg | | 82.329(1) | 88.790(1) |
| $V$, Å$^3$ | 7119(2) | 3521.12(9) | 1797.04(6) |
| $Z$ | 8 | 4 | 2 |
| $D$ (calcd), g cm$^{-3}$ | 1.692 | 1.794 | 1.845 |
| $\mu$, mm$^{-1}$ | 2.712 | 3.800 | 3.471 |
| diffractometer | Smart CCD | Kappa CCD | Kappa CCD |
| radiation ($\lambda$), Å | 0.71073 | 0.71073 | 0.71073 |
| temperature, K | 298(2) | 200(2) | 200(2) |
| $\theta$ range for collection, deg | 2.09−24.98 | 2.09−25.39 | 2.16−25.37 |
| $T_{min}/T_{max}$ | 0.59/0.64 | 0.31/0.41 | 0.35/ 0.72 |
| no. of independent reflections ($I > 2\sigma(I)$) | 8874 ($R_{int}$ = 0.0253) | 8626 ($R_{int}$ = 0.0717) | 5676 ($R_{int}$ = 0.0348) |
| no. of parameters | 731 | 751 | 374 |
| R1[a]/wR2[a] ($I > 2\sigma(I)$) | 0.040/0.086 | 0.050/0.124 | 0.053/0.153 |
| R1[a]/wR2[a] (all data) | 0.058/0.092 | 0.088/0.146 | 0.061/0.160 |

| | $[Et_4N]_2$[**2a**] | $[Et_4N]_2$[**3b**] | $[Et_4N]_2$[**3c**] | $[Et_4N]_2$[**4a**] |
|---|---|---|---|---|
| empirical formula | $C_{25}H_{40}Cl_2Cu_2Fe_3N_2O_9Te$ | $C_{34}H_{40}BrCu_3Fe_6N_2O_{18}Te_2$ | $C_{34}H_{40}ICu_3Fe_6N_2O_{18}Te_2$ | $C_{34}H_{40}Cl_2Cu_4Fe_6N_2O_{18}Te_2$ |
| formula weight | 1005.72 | 1625.51 | 1672.50 | 1680.04 |
| crystal system | monoclinic | monoclinic | monoclinic | monoclinic |
| space group | $P2_1/n$ | $P2/c$ | $P2_1/a$ | $P2_1/n$ |
| crystal dimensions, mm | 0.40 × 0.18 × 0.10 | 0.13 × 0.05 × 0.02 | 0.18 × 0.14 × 0.05 | 0.14 × 0.10 × 0.03 |
| $a$, Å | 11.1306(2) | 17.5999(3) | 13.5631(2) | 11.7406(3) |
| $b$, Å | 14.5567(3) | 8.9940(1) | 21.7605(4) | 17.8279(5) |
| $c$, Å | 22.3697(5) | 32.2236(6) | 17.2648(3) | 12.3063(4) |
| α, deg | | | | |
| $\beta$, deg | 96.307(1) | 96.358(1) | 98.830(1) | 92.422(1) |
| $\gamma$, deg | | | | |
| $V$, Å$^3$ | 3602.8(1) | 5069.4(1) | 5035.1 (2) | 2573.6(1) |
| $Z$ | 4 | 4 | 4 | 2 |
| $D$ (calcd), g cm$^{-3}$ | 1.854 | 2.130 | 2.206 | 2.168 |
| $\mu$, mm$^{-1}$ | 3.330 | 4.879 | 4.732 | 4.537 |
| diffractometer | Kappa CCD | Kappa CCD | Kappa CCD | Kappa CCD |
| radiation ($\lambda$), Å | 0.71073 | 0.71073 | 0.71073 | 0.71073 |
| temperature, K | 100(2) | 200(2) | 200(2) | 298(2) |
| $\theta$ range for collection, deg | 2.14−25.02 | 2.26−25.36 | 2.22−25.33 | 2.01−25.00 |
| $T_{min}/T_{max}$ | 0.43/0.53 | 0.63/0.92 | 0.63/0.77 | 0.63/0.73 |
| no. of independent reflections ($I > 2\sigma(I)$) | 5181 ($R_{int}$ = 0.0597) | 5950 ($R_{int}$ = 0.1055) | 7121 ($R_{int}$ = 0.0754) | 3663 ($R_{int}$ = 0.0625) |
| no. of parameters | 398 | 595 | 595 | 298 |
| R1[a]/wR2[a] ($I > 2\sigma(I)$) | 0.041/0.100 | 0.067/0.167 | 0.047/0.121 | 0.063/0.164 |
| R1[a]/wR2[a] (all data) | 0.059/0.127 | 0.115/0.207 | 0.073/0.152 | 0.086/0.195 |

[a] The functions minimized during least-squares cycles were $R1 = \sum||F_o| - |F_c||/\sum|F_o|$ and $wR2 = [\sum w(F_o^2 - F_c^2)^2/\sum w(F_o^2)^2]^{1/2}$.

representations of the molecular orbitals were obtained using CS Chem3D 5.0.

**Electrochemical Measurements.** The cyclic voltammetry measurements were performed at the room temperature under a nitrogen atmosphere and recorded using a BAS-100W electrochemical potentiostat. A platinum disk working electrode, a platinum wire auxiliary electrode, and a non-aqueous $Ag/Ag^+$ electrode were used in a three-electrode configuration. Tetra-*n*-butylammonium perchlorate (TBAP) was used as the supporting electrolyte, and the solute concentration was $\sim 10^{-3}$ M. The redox potentials were calibrated with a ferrocenium/ferrocene ($Fc^+$/Fc) couple in the working solution and referenced to SCE.

**Acknowledgment.** This work was supported by the National Science Council of Taiwan (NSC 95-2113-M-003-009-MY3 to M. Shieh) and National Taiwan Normal University. We are also grateful to the National Center for High-Performance Computing, where the Gaussian package and computer time were provided. Our gratitude also goes to the Academic Paper Editing Clinic, NTNU.

**Supporting Information Available:** X-ray crystallographic files in CIF format for $[Et_4N]_2$[**1a**], $[Et_4N]_2$[**1b**], $[Et_4N]_2$[**1c**], $[Et_4N]_2$[**2a**], $[Et_4N]_2$[**3b**], $[Et_4N]_2$[**3c**], and $[Et_4N]_2$[**4a**]. Computational details for complexes **1a**−**1c**, **2a**−**2c**, **2a′**−**2c′**, **3a**−**3c**, **4a**−**4c**, and $[TeFe_3(CO)_9]^{2-}$. This material is available free of charge via the Internet at http://pubs.acs.org.